Acta Pharmaceutica Sinica B 2020;10(11):2227–2245

Chinese Pharmaceutical Association
Institute of Materia Medica, Chinese Academy of Medical Sciences

Acta Pharmaceutica Sinica B

www.elsevier.com/locate/apsb
www.sciencedirect.com

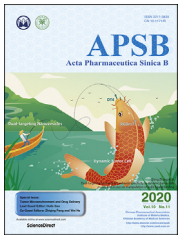

ORIGINAL ARTICLE

Injectable thermo-responsive nano-hydrogel loading triptolide for the anti-breast cancer enhancement *via* localized treatment based on "two strikes" effects

Yaoyao Luo[a,†], Jingjing Li[b,†], Yichen Hu[c], Fei Gao[a], George Pak-Heng Leung[b], Funeng Geng[a,d], Chaomei Fu[a,*], Jinming Zhang[a,*]

[a]*College of Pharmacy, Chengdu University of Traditional Chinese Medicine, Chengdu 611137, China*
[b]*Department of Pharmacology and Pharmacy, University of Hong Kong, HongKong 999077, China*
[c]*College of Pharmacy and Biological Engineering, Chengdu University, Chengdu 610100, China*
[d]*Sichuan Key Laboratory of Medical American Cockroach, Chengdu 615000, China*

Received 31 January 2020; received in revised form 25 March 2020; accepted 27 March 2020

KEYWORDS

Thermo-responsive hydrogel;
Triptolide;
Tumor local treatment;
Breast cancer;
Anti-angiogenesis;
Pro-apoptosis;
Micelle;
Survival rate

Abstract The clinical application of triptolide (TPL) in tumor therapy has been greatly limited by its toxicity and inefficient delivery. Herein, a localized and sustained-release thermo-sensitive hydrogel was developed for the intra-tumor administration of TPL. Based on the amphiphilic structure of poly (*N*-isopropylacrylamide-*co*-acrylic acid)-*g*-F68 copolymer, it was able to form nano-micelles to efficiently encapsulate TPL, and then turn into a hydrogel at 37 °C. TPL@nano-gel exhibited a sustained drug release profile *in vitro* and a stronger anticancer effect caused by "two strikes". The "first strike" was its enhanced cytotoxicity compared to free TPL, due to the enhanced pro-apoptosis effect observed in both MDA-MB-231 and MCF-7 cells caused by the regulation of endogenous mitochondrial pathways. Furthermore, TPL@nano-gel exhibited a "second-strike" through its anti-angiogenesis capabilities mediated through VEGFR-2 signaling inhibition. As expected, after intra-tumoral injection at a 0.45 mg/kg TPL-equivalent dose three times over 14 days in 4T1 tumor-bearing mice, TPL@nano-gel led to lower systemic toxicity and higher antitumor efficacy compared to multiple injections of TPL. In this regard,

*Corresponding authors. Tel.: +86 028 61800231 (Chaomei Fu); +86 13551043885 (Jinming Zhang).
E-mail addresses: chaomeifu@126.com (Chaomei Fu), cdutcmzjm@126.com (Jinming Zhang).
†These authors made equal contributions to this work.
Peer review under the responsibility of Institute of Materia Medica, Chinese Academy of Medical Sciences and Chinese Pharmaceutical Association.

https://doi.org/10.1016/j.apsb.2020.05.011

these findings indicate that this injectable thermo-responsive hydrogel carries great potential for TPL as a safe and effective cancer therapy.

1. Introduction

Triptolide (TPL) is a diterpenoid triepoxide isolated from *Tripterygium wilfordii.* Hook F, commonly known as "Thunder God Vine" or "Lei Gong Teng", whose highly effective anticancer activity has been reported for many types of cancers[1,2]. Increasing experimental evidence suggests its broad antitumor capacity involves various mechanisms[3]. The promising anti-tumor activities of TPL, however, have been hindered by significant challenges in practice due to its narrow therapeutic window, poor water solubility, and multi-organ toxicity. To avoid the adverse effects in normal cells and tissues caused by systemic administration, localized drug delivery[4,5] could be employed. This would not only limit rapid drug clearance and minimize systemic side effects, but also improve its anticancer efficacy by promoting localized and sustained drug release in the tumor tissue[6]. Injectable nanometer-sized hydrogels with 3D networks have been widely utilized as site-specific drug delivery systems due to their hydrophilicity, flexibility, versatility, biocompatibility, tunable morphology, and tailored surface properties[7,8]. Particularly, stimulus-responsive hydrogels for intra-tumor injection enable high-dose tumor-specific drug delivery, as well as abrupt changes in volume in response to environmental factors[9].

Thermo-responsive hydrogels have been widely utilized in tumor treatment[10]. Biodegradable and biocompatible poly (*N*-isopropylacrylamide) (PNIPAM), with a lower critical solution temperature (LCST) of about 32 °C and thermo-reversible gelation traits that enable it to form a liquid at room temperature and a gel at body temperature, is one of the most well-studied thermo-responsive polymers[11]. The phase transition temperature, mechanical strength, and biocompatibility of this hydrogel can be regulated through the use of chemical cross-linking to natural polysaccharides and other polymers to form PNIPAM copolymers[12−15]. However, drugs loaded in thermo-responsive hydrogels commonly suffer from an uncontrolled initial burst release followed by a subsequent gradual release. Cisplatin-loaded hydrogel formulations based on simple physical encapsulation were reported to exhibit a burst effect, commonly observed to last only a few hours[16]. Furthermore, hydrophobic drugs such as PTX exhibited a sustained release from the hydrogel matrix for over one month[17], which caused localized tissue irritation, pain, and toxicity due to the high local drug concentration[18], as well as insufficient anticancer efficacy because of the low cellular drug concentration.

To help remedy this issue, this study sought to develop an optimal injectable hydrogel carrier, which could not only provide sustained diffusion and degradation at the tumor site, but could also improve the cellular uptake and intracellular drug release in cancer cells. To accomplish this, we synthesized a novel dual stimuli-responsive poly (*N*-isopropylacrylamide-*co*-acrylic acid)-*g*-pluronic F68 [p (NIPAAm-*co*-AAc)-*g*-F68] hydrogel for TPL localized treatment. In this complex copolymer, pH-sensitive acrylic acid monomer was blocked on PNIPAM by atomic transfer radical polymerization in response to the acidic microenvironment in cancer cells due to protonation of the carboxylate groups[19]. Pluronic F68 was grafted on the PNIPAM polymer backbone to regulate LCST and improve the sustained diffusion properties of the hydrogel[20]. The p (NIPAAm-*co*-AAc)-*g*-F68 copolymers could self-assemble into stable, dual temperature- and pH-responsive micelles with uniform sizes, and were able to efficiently encapsulate TPL. The single injection of TPL/p (NIPAAm-*co*-AAc)-*g*-F68 solution could produce improved anticancer effects due to the advantages of the dual stimuli-responsive nano-hydrogel in combination with the cytotoxicity and anti-angiogenesis activity of TPL, as illustrated in Scheme 1. Finally, we determined the enhanced antitumor efficacy of this TPL-loaded hydrogel *in vitro* and *in vivo*.

2. Materials and methods

2.1. Materials and methods

N-Isopropylacrylamide (NIPAM) was purchased from Chengdu Huaxia Chemical Reagent Co. Ltd. (Chengdu, China). Acrylic acid (AAc), potassium persulfate (KPS) and *N*,*N*,*N*′,*N*′-tetramethylethylenediamine (TEMED) were purchased from Chengdu Kelong Chemical Reagent Co. Ltd. (Chengdu, China). Pluronic F68, 1-(3-dimethylaminopropyl)-3-ethylcarbodiimide hydrochloride (EDC), and 4-(dimethylamino)-pyridin (DMAP) were purchased from Aladdin Biochemical Technology Co. Ltd. (Shanghai, China). Triptolide (TPL) was purchased from Chengdu Desita Biological Technology Co. Ltd. (Chengdu, China). Dimethyl sulfoxide (DMSO), heparin, gelatin, collagen, protease, endothelial cell growth supplement, 3-(4,5-dimethylthiazol-2-yl)-2,5-diphenyltetrazoliumbromide (MTT), and Drabkin reagent Kit 525 were purchased from Sigma−Aldrich (St. Louis, USA). Dulbecco's modified Eagle's medium (DMEM), fetal bovine serum (FBS), phosphate-buffered saline (PBS), penicillin−streptomycin, and 0.25% (*w*/*v*) trypsin containing 1 mmol/L EDTA were purchased from Invitrogen (Carlsbad, USA). Growth factor reduced matrigel was supplied by BD Biosciences (Franklin Lakes, USA). Recombinant human vascular endothelial cell growth factor (VEGF) 165 proteins were obtained from R&D systems (Minneapolis, USA). The lactate dehydrogenase (LDH) cytotoxicity assay kit was purchased from Cayman Chemical (Ann Arbor, USA). Caspase 3/7 activity kit was obtained from Promega Corporation (Madison, USA). VEGF-A ELISA kit was obtained from Abcam (Cambridge, USA). All the antibodies were purchased from Cell Signaling Technology (Danvers, USA). All chemicals were dissolved in appropriate solvents and stored at −20 °C before use for maintaining the chemical stability. Male BALB/c nude mice, aged 4−6-week old and male Sprague−Dawley rats, aged 6−8-week old were

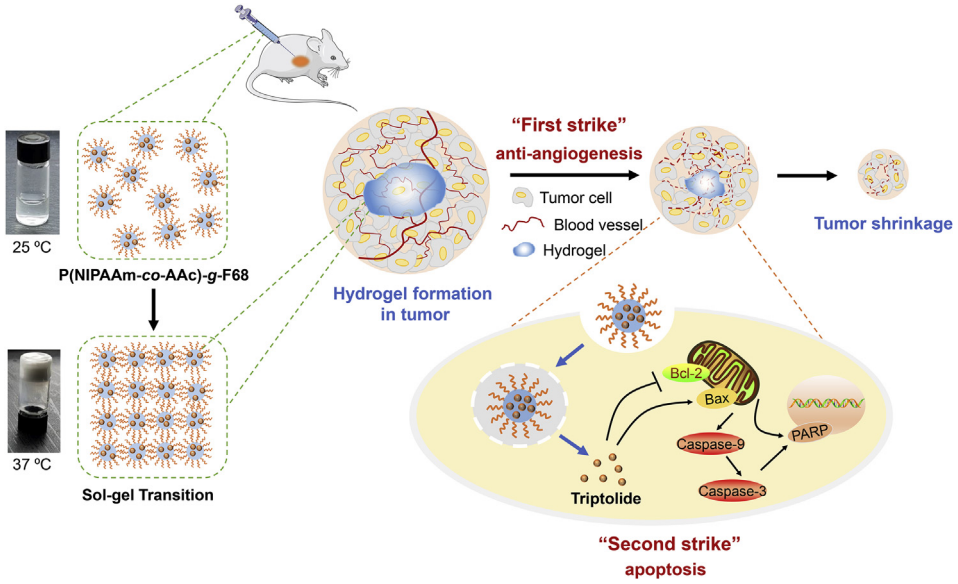

Scheme 1 Schematic illustration of injectable thermosensitive nano-hydrogel loading triptolide (TPL) composed by the self-assembly of p(NIPAAm-*co*-AAc)-*g*-F68 copolymer for localized tumor therapy, mediated by two strike approaches: anti-angiogenesis and cancer cell apoptosis.

supplied by Chengdu Dashuo Biological Technology Co. Ltd. (Chengdu, China). All animal experiments were performed according to the rules of Experimental Animals Administrative Committee of Chengdu University of Traditional Chinese Medicine (Chengdu, China).

2.2. *Synthesis of poly (N-isopropylacrylamide-co-acrylic acid)*

Poly (*N*-isopropylacrylamide-*co*-acrylic acid) [p (NIPAAm-*co*-AAc)] polymers were synthesized by free radical polymerization of NIPAM monomers and AAc with KPS as an initiator at 75 °C. Briefly, 60 mL of deionized water was deoxidized by N_2 bubbling for 15 min. NIPAM monomer (2 g, 17.67 mmol) was then dissolved in deionized water. Subsequently, AAc (1.58 g, 21.92 mmol), KPS (0.06 g, 0.22 mmol) and TEMED (0.388 g, 3.34 mmol) were added into the solution with stirring at 75 °C in oil bath for 24 h. It clearly can be seen that the colorless and transparent mixed solution turns into a sky blue and finally becomes a milky white, which indicating that the polymerization was successful. After the polymerization, the polymer was washed with water and anhydrous ethanol several times to remove the unreacted monomer and other impurities by centrifuge. Reaction crudes were was dried overnight at 40 °C and stored at 4 °C.

2.3. *Synthesis of p(NIPAAm-co-AAc)-g-F68 copolymer*

The collected p(NIPAAm-*co*-AAc) polymer (0.5 g) and EDC (0.12 g, 0.63 mmol) were dissolved in 15 mL DMF together with stirring for 2 h to activate carboxyl group. Then, DMAP (0.07 g, 0.57 mmol) and 0.1 g of F68 were added into the mixture and reacted continuously for 24 h with a magnetic stirring bar. The polymer solution was further dialyzed against distilled water (MWCO of 2000 kDa dialysis tubes) for 3 days to remove unreacted substance. The p(NIPAAm-*co*-AAc)-*g*-F68 copolymer was then lyophilized and stored at room temperature in a desiccator.

2.4. *Structural characterization of p(NIPAAm-co-AAc)-g-F68 copolymer*

^{1}H NMR spectrometry (AVANCE III HD 500 MHz spectrometer; Bruker, Germany) was used to characterize the synthesized p(NIPAAm-*co*-AAc)-*g*-F68 copolymer with DMSO-d_6 as the solvent. Additionally, Fourier transform infrared (FT-IR) was used to compare the structural difference of p(NIPAAm-*co*-AAc)-*g*-F68, p(NIPAAm-*co*-AAc) and F68. The FT-IR spectra recorded using KBr disks on FT-IR spectrometer (Shimadzu IRTracer-100, Kyoto, Japan) in the range of 4000−400∼ cm^{-1}. Furthermore, the molecular weight of p(NIPAAm-*co*-AAc)-*g*-F68 was determined by gel permeation chromatography (GPC), performed with 18-angle laser light scattering gel permeation chromatography system equipped with Shodex OHpak SB-806HQ (Shodex, Tokyo, Japan) connected Tandem connection and Shimadzu RID-10 A refractive index detector. Ultrapure water (0.02% sodium azide, pH 6.0) was used as the mobile phase at a flow rate of 1 mL/min at 25 °C. Number molecular weights (M_w), weight average molecular weights (M_n) and a molecular weight polydispersity index (M_w/M_n) were determined.

2.5. *Lower critical solution temperature (LCST) value of p(NIPAAm-co-AAc)-g-F68 copolymer*

P(NIPAAm-*co*-AAc)-*g*-F68 copolymer was swelled fully in deionized water at concentrations of 5% (*w*/*v*) under 4 °C. The temperature dependence absorbance value at 470 nm was determined using an UV−Vis spectrophotometer (Helios alpha,

Thermo Spectronic, Boston, USA) equipped with an oil bath to control temperature from 25 to 40 °C. The LCST value was defined as the temperature at which the optical absorbance increased around 50% in comparison to initial absorbance[25].

2.6. Critical micellar concentration value of p(NIPAAm-co-AAc)-g-F68 copolymer

The critical micellar concentration (CMC) value of p(NIPAAm-*co*-AAc)-*g*-F68 copolymer was determined by the standard pyrene method as a fluorescence probe[26]. The intensity ratios at 373 and 384 nm (I_{373}/I_{384}) were analyzed and plotted against the logarithm of the concentration. The CMC value was the point of intersection of two straight lines.

2.7. Sol−gel transition and rheological property

The tube-inverting method was used to determine the sol−gel transition temperature of polymer aqueous solution. Dynamic rheological properties of polymer solutions were investigated using a dynamic stress-controlled rheometer. The viscosity of the aqueous polymer solution was measured using an Anton Paar Physica MCR 302 rheometer (Graz, Austria) with a Peltier controller with plate geometry (Ø 25 mm). The viscosity data was recorded at a continuously increasing temperature from 20 to 70 °C at a rate of 1 °C/min[27].

2.8. Preparation of TPL-loaded nano-micelles in hydrogel

Typically, 30 mg p(NIPAAm-*co*-AAc)-*g*-F68 copolymer and 2 mg TPL were dissolved in 2 mL of acetone together, with the assistance of sonication dispersion at the power of 90 W for 60 s. And then, the mixture was gently dropped to 10 mL of deionized water phase with a stirring for 5 h at room temperature to evaporate the residual acetone. Owing to the amphiphilic structure of p(NIPAAm-*co*-AAc)-*g*-F68 copolymer, the TPL hydrogel were prepared by a solvent evaporation method. Finally, free TPL drugs were removed by filtered by 0.45 μm micro-porous membrane. The TPL hydrogel supernatant was stored at 4 °C before use.

To determine the drug loading efficiency (DLE) and drug entrapment efficiency (DEE) in hydrogel, 1 mg of lyophilized TPL hydrogel was dissolved in 4 mL of methanol with ultrasonication for 2 min. The concentration of TPL was tested by HPLC analysis (Waters ACQUITY UPLC®, Milford, US) with the mobile phase of methanol: water (46%:54%) at 220 nm, using a previously established standard calibration curve. The DLE and DEE were calculated as following formulas Eqs. (1) and (2):

$$\text{DEL}\ (\%) = \frac{\text{Amount of drug in nanogel}}{\text{Amount of total fed}} \times 100 \quad (1)$$

$$\text{DEE}\ (\%) = \frac{\text{Amount of drug in nanogel}}{\text{Amount of drug fed} - \text{unloaded drug}} \times 100 \quad (2)$$

2.9. Characterization of TPL-loaded nano-micelles in hydrogel

The size and zeta-potential of TPL hydrogel were analyzed by a Malvern Zetasizer (Nano ZS90, Malvern Instruments, UK) at room temperature. The morphology of NPs in hydrogel was observed by JEOL 2010 high-resolution transmission electron microscopy (JEOL, Tokyo, Japan) with an accelerating voltage of 200 kV. The surface morphology of hydrogels was studied by field emission scanning electron microscopy (SEM), using S4800 equipment (Hitachi, Tokyo, Japan) with an operating voltage of 5 kV. Briefly, hydrogel sample was quickly frozen in liquid nitrogen and then lyophilized for 48 h. The freeze-dried hydrogel was fixed on brass holders and coated by sputtering with a thin Au layer[28].

Additionally, the thermal analysis of hydrogel was analyzed using X-ray diffraction (XRD), and differential scanning calorimetry (DSC, American TA Company Q2000) to examine the crystal form transfer during encapsulation. Respectively, XRD analysis was performed on a diffractometer (Bruker D8 Advance, Germany) operating with a CuK source in the range of 25−70 °C at a speed of 1 °C/min. DSC curves were determined under dry N_2 atmosphere (flow of 20 mL/min) ranging from 30 to 250 °C.

2.10. In vitro drug release of TPL from hydrogel

Typically, 2 mL of TPL@nano-solution freshly prepared was injected to a dialysis tubing (MWCO of 3000 Da), immersed into 50 mL of PBS buffer [pH 7.4, containing 0.5% (*w*/*w*) Tween 80 and 0.025% (*w*/*w*) NaN_3] and then incubated in a shaking bath (100 rpm) at 25 and 37 °C, respectively. At scheduled time intervals, 2 mL of the release medium was withdrawn and then replaced with an equal volume of fresh medium periodically[29]. The TPL concentration in the release medium was determined by HPLC (Agilent Technology, 1100 series, Santa Clara, United States), equipped with a C18 column and a UV detector. The mobile phase was methanol/water (46:54, *v*/*v*) and UV absorbance was detected at a wavelength of 220 nm at 25 °C.

2.11. Cell culture

Human umbilical vein endothelial cells (HUVECs), human breast cancer cells (MDA-MB-231 and MCF-7) and mouse breast cancer cells (4T1) were obtained from American Type Culture Collection (Manassas, USA). HUVECs were cultured in vascular cell basal medium supplemented with 10 mmol/L L-glutamine, 1 μg/mL hydrocortisone hemisuccinate, 50 μg/mL ascorbic acid, 100 μg/mL heparin, 30 μg/mL endothelial cell growth supplement, 10% heat-inactivated FBS, and 1% penicillin–streptomycin. Cells at early passage (3−8 passages) were used in all experiments. Tissue flasks were pre-coated with 0.1% gelatin before HUVECs culturing. On the other hand, MDA-MB-231, MCF-7 and 4T1 breast cancer cells were cultured in DMEM supplemented with 10% heat-inactivated FBS and 1% penicillin–streptomycin. All the cells were incubated at 37 °C in a humidified atmosphere with 5% CO_2.

2.12. Cell viability of breast cancer cells by MTT assay

Human breast cancer cells (MDA-MB-231 and MCF-7) were seeded into 96-well plates at a density of 5×10^3 cells/well and cultured for 24 h for cell attachment. Cells were then treated with various concentrations (0−160 nmol/L) of free TPL and TPL@nano-gel in low serum media (0.5% FBS) for 24 or 48 h. Cells treated with 0.1% DMSO served as negative control. Cell viability was measured with the MTT assay according to the manufacturer's protocol.

2.13. Mitochondrial membrane potential (MMP) assay

MDA-MB-231 and MCF-7 human breast cancer cells were seeded into 12-well plates at a density of 2×10^5 cells/well for 24 h, and then incubated in low serum medium containing blank gel, free TPL (20 nmol/L) and TPL@nano-gel (20 nmol/L) for 24 h. After treatment, cells were collected and incubated with JC-1 dye (3 μg/mL) for 20 min at 37 °C in a CO_2 incubator. The cells were subsequently washed twice with PBS and examined by flow cytometry with 10,000 gated cells. For signal quantification, the intensity of red fluorescence (excitation 560 nm, emission 595 nm) and green fluorescence (excitation 485 nm, emission 535 nm) was determined. The ratio of red/green fluorescence was calculated for semi-quantitative assessment of mitochondrial polarization states.

2.14. Cell apoptosis analysis by Annexin V-FITC/PI double staining

MDA-MB-231 and MCF-7 human breast cancer cells were seeded into 12-well plates at a density of 2×10^5 cells/well for 24 h, and then incubated in low serum medium-containing blank gel, free TPL (20 nmol/L) and TPL@nano-gel (20 nmol/L) for 48 h. At the end of the incubation, cells were washed twice with cold PBS, harvested, resuspended in binding buffer, and stained with Annexin V-FITC and PI (1.0 mg/mL) for 15 min. The stained cells were analyzed immediately using a flow cytometer (BD Biosciences, Franklin Lakes, USA)[30]. Ten thousand events were counted for each sample. The data were analyzed using FlowJo software (BD Biosciences, New York, USA).

2.15. Cell cycle analysis

MDA-MB-231 and MCF-7 human breast cancer cells were seeded into 12-well plates at a density of 2×10^5 cells/well. After 48 h of blank gel, free TPL (20 nmol/L) and TPL@nano-gel (20 nmol/L) treatment, cells were fixed with 70% ethanol overnight at −20 °C and stained with PI (1.0 mg/mL) in the presence of RNase A (200 μg/mL) for 15 min at room temperature. The samples were then analyzed using the PE channel of flow cytometry (BD Biosciences).

2.16. Western blotting assay to detect protein expression

After MDA-MB-231 and MCF-7 cells from each treatment group were harvested, the cells were lysed, sonicated on ice for 20 min, and mixed with RIPA buffer containing protease and phosphorylase inhibitors (Sigma−Aldrich). The lysates were centrifuged at 12,000 rpm for 15 min using BECKMAN COULTER Microfuge 22 R centrifuge (Brea, US), and the supernatants were collected and analyzed with a BCA Protein Assay Kit. The protein samples were stored at −20 °C until usage.

Equal amounts of protein were subjected to sodium dodecyl sulfate-polyacrylamide gel electrophoresis, and then electrically transferred onto a polyvinylidene difluoride membrane, which was subsequently blocked with 5% non-fat milk in Tris-buffered saline containing 0.1% Tween-20 for 1 h. The membrane was subsequently incubated with primary antibodies against PARP, cleaved-PARP, cleaved-caspase 3, cleaved-caspase 9, BAX, BCL-2, cyclin D1, or GAPDH overnight at 4 °C. The membranes were washed four times with Tris-buffered saline-Tween (TBST) and incubated with a secondary antibody at room temperature for 1 h. Images of protein bands were captured, and densitometric measurements of band intensity were performed using the Molecular Imager ChemiDoc XRS (Bio-Rad Laboratories, Hercules, USA).

2.17. Caspase-glo 3/7 and VEGF activity in cancer cells

MDA-MB-231 and MCF-7 human breast cancer cells were treated with blank gel, free TPL (20 nmol/L) and TPL@nano-gel (20 nmol/L) for 48 h 100 μL of caspase 3/7 reagent were added to each well, mixed and incubated for 1 h at room temperature, respectively. The activity of caspase 3/7 was measured using a commercial kit according to manufacturer's instructions, and expressed as percentage of the negative control. Moreover, the secreted VEGF-A levels of MDA-MB-231 and MCF-7 cell culture medium were measured, after cells treated by various agents as above-mentioned. The level of VEGF in cancer cells was quantified using a commercial ELISA kit according to manufacturer's instructions.

2.18. HUVECs cell proliferation assay

HUVECs were seeded into 48-well plates at a density of 3×10^4 cells/well and cultured for 24 h for cell attachment. Primarily, the cell cytotoxicity of TPL formulations with the TPL concentration ranging from 0 to 40 nmol/L for 48 h treatment was evaluated by MTT assay. Subsequently, cells were then starved with low serum media overnight to achieve a quiescent state. After starvation, the cells were treated with various concentrations (0−20 nmol/L) of free TPL and TPL@nano-gel in low serum media containing VEGF (20 ng/mL) for 48 h. Cells treated with 0.1% DMSO and VEGF served as negative control and positive control, respectively. After treatment, cell proliferation was determined using a BrdU Cell Proliferation Kit (Millipore, Billerica, USA), following the manufacturer's instructions.

2.19. Transwell migration and invasion assay

Cell migration and invasion assays in HUVECs were performed as described in a previous study[31]. In the cell migration assay, the upper and lower sides of the Transwell membrane (8 μm pores) were pre-coated with 0.1% collagen. In the invasion assay, the upper and lower sides of the membrane were pre-coated with 100 μL matrigel (20% in blank medium). HUVECs were seeded into the Transwells at a density of 5×10^4 cells/well and cultured in low serum medium containing VEGF (20 ng/mL) and 10 nmol/L of free TPL and TPL@nano-gel. Cells were incubated for 24 h at 37 °C, and the cells on the upper surface of the Transwell membrane were then removed using cotton swabs. The Transwell membranes were fixed with 4% paraformaldehyde for 15 min, and then stained with Hoechst 33,342 (10 μg/mL) for 15 min. The membranes were then mounted on microscope slides and images were captured using a fluorescence inverted microscope and a charge-coupled device camera (AxioCam HRC, Carl Zeiss, Oberkochen, Germany). Cell migration and invasion were quantified by counting the number of cells per insert using ImageJ software (National Institutes of Health, Bethesda, USA).

2.20. VEGF-mediated signaling pathway analysis by Western blot

To assess the inhibitory effects of TPL@nano-gel on the VEGF-mediated signaling pathways *via* the receptors that are expressed on HUVECs, the amount of VEGFR2, p-VEGFR2, AKT, p-AKT, mTOR, p-mTOR, ERK1/2, p-ERK1/2, P38, p-P38, eNOS and p-eNOS was analyzed using the Western blot analysis as described above. The transferred proteins were visualized using an enhanced chemiluminescent detection kit.

2.21. Rat aortic ring sprouting assay

Aorta ring sprouting assay was performed as described previously[32]. Aortic rings isolated from 6- to 8-week-old male Sprague−Dawley rats, then cleaned off periadventitial fat and cut into 1.5 mm size. Aortas were rinsed by cold PBS for at least three times, then quickly moved into the well and overlaid with 100 μL of matrigel for sealing. Serum-free culture medium containing VEGF (100 ng/mL), with or without TPL formulations containing 20 nmol/L of TPL, was added to the wells. The medium was changed every two days. After 10 days, the micro-vessel growth was photographed by an inverted microscope and the number of branching sites was quantified by ImageJ software.

2.22. VEGF-induced angiogenesis matrigel plug assay

The angiogenesis matrigel plug assay with BALB/c mice as described previously[33] was used to determine *in vivo* anti-angiogenic effects of TPL@nano-gel. Growth factor-reduced matrigel 0.5 mL containing heparin (100 units) and VEGF (250 ng) with or without TPL@nano-gel containing 20 nmol/L of TPL was subcutaneously injected into ventral area of 6-week-old male BALB/c mice ($n = 5$). After 14 days of implantation, mice were sacrificed, and the matrigel plugs were removed. To quantify the formation of functional blood vessels, the amount of hemoglobin was measured by using Drabkin reagent Kit 525.

2.23. Intra-tumoral retention of fluorescence-labeled gel by IVIS spectrum

0.1 mL of 4T1 cells suspension (5×10^6 cells/mL) was injected into the right upper limb of female BALB/c mice. When the tumor volume reached ~1000 mm^3, both Cy5-labeled hydrogel (certain amount of Cy5 was added into micelle solution and solidified into hydrogel) and free Cy5-suspended saline containing 1% Tween-80 were respectively injected into tumor tissue directly (50 μL, single dose), respectively. At predetermined time intervals, *i.e.*, 4, 8, 12, 24, 48 and 72 h after injection, mice were anesthetized with 0.2 mL 4% chloral hydrate and then photographed using an IVIS Lumina Series III imaging system (PerkinElmer, Waltham, USA)[34]. Meanwhile, mice were sacrificed at 24 and 48 h post-injection. The main organs including heart, liver, spleen, lung, kidney, and tumor were harvested and photographed under the fluorescence imaging view.

2.24. In vivo tumor inhibition effect of TPL@nano-gel

The subcutaneous dorsa of BALB/c mice (4 weeks old) were inoculated with mouse 4T1 breast cancer cells (5×10^6 cells/mouse). Tumors were allowed to grow to approximately 200 mm^3. The xenograft mice were then randomly assigned to four groups and injected intra-tumorally at Days 1, 5 and 10 with saline, blank gel, free TPL and TPL@nano-gel (0.45 mg/kg). The body weight and tumor volume ([width]^2 × [length]/2) were recorded once every 2 days. At Day 14, parts of mice (6 mice in each group) were then sacrificed and photographed, and the primary tumors were excised and weighted. The tumor tissues were fixed with 4% (*v*/*v*) formaldehyde and sectioned into 6 μm slices. Tumor and major organs sections were stained with hematoxylin and eosin to examine tissue morphology. Tumor sections were also stained with primary antibodies against VEGF, CD31 and Ki-67 to evaluate angiogenesis and cell proliferation in tumor tissue. Western blot assay was performed to evaluate the expression of some apoptosis-related proteins in tumor tissue, *i.e.*, PARP, cleaved-PARP, cleaved-caspase 3, cleaved-9, BAX, and BCL-2. In addition, survival rate of mice in each group were observed sequentially. The mean survival time and percentage increased life span were calculated on the basis of mortality of the experimental mice ($n = 10$) in solid tumor. Survival curves were generated using a threshold aggregate tumor burden per mouse of 2000 mm^3, which was used as a proxy for survival. Data from tumors exceeding this burden were not censored from the tumor growth curves.

2.25. Statistical analysis

Data are expressed as the mean ± Standard deviation (SD) of at least three independent experiments. Data were analyzed by Graph Pad Prism 5.0 (La Jolla, USA). Statistical significance was determined by one-way analysis of variance, and a P value < 0.05 was considered significant.

3. Results and discussion

3.1. Copolymer synthesis and characterization

To prepare the thermo-responsive hydrogel, p(NIPAAm-*co*-AAc)-*g*-F68 polymer was synthesized by free radical polymerization of NIPAM monomers and AAc, using KPS as initiator and TEMED as accelerator, and then grafted to Pluronic F68 mediated by the esterification reaction. The synthesized route was shown in Fig. 1A. The successful grafting was demonstrated by changes in the ^{1}HNR and FT-IR spectra. The ^{1}H NRM spectra of p(NIPAAm-*co*-AAc)-*g*-F68 copolymer is displayed in Fig. 1B, where the proton signals can be recognized. The signals for the −CH and $-CH_2$ groups on the main chain of Pluronic F68 (H8'+H9'+H10′), located around 3.65 ppm, could be found in both (a) and (c). The other alkyl −CH and $-CH_2$ protons (H4'+H5'+H6'+H7′) in the copolymer appeared as multiples at 1.2−2 ppm, which were derived from the PNIPAM monomer. The peak at 7.14 ppm represents the amide group (H3') proton in the PNIPAM monomer[21]. Therefore, the observed characteristic resonances of p(NIPAAm-*co*-AAc)-*g*-F68 copolymer validate the success of the synthesis process.

Moreover, the grafting process could be confirmed by the FT-IR spectra of F68, p(NIPAAm-*co*-AAc), and the pNIPAAm-*co*-AAc)-*g*-F68 polymer. As shown in Fig. 1C, some characteristic absorption bands derived from Pluonic F68 and P (NIPAAm-*co*-AAc) could be observed in the spectrum of p(NIPAAm-*co*-AAc)-*g*-F68, such as the characteristic amide bands at 1645 and 1532 cm^{-1}, and the two isopropylmethyl groups at 1366 and 1386 cm^{-1} from PNIPAM[22]. Meanwhile, some characteristic

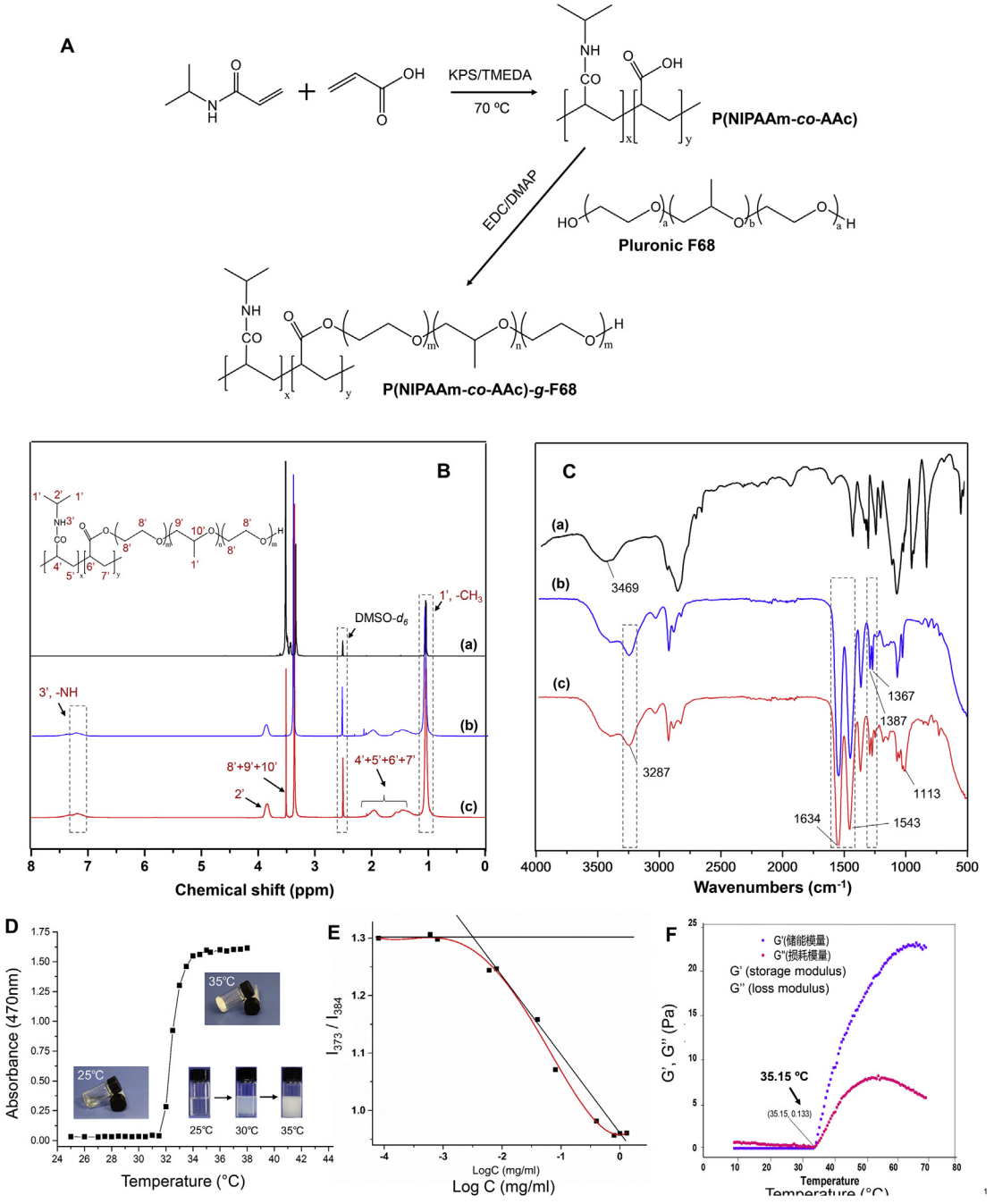

Figure 1 (A) Synthesis scheme of the p (NIPAAm-*co*-AAc)-*g*-F68 copolymer. ^{1}H NMR spectra (B) and FT-IR spectra (C) of F68 (a), p (NIPAAm-*co*-AAc) (b), and p (NIPAAm-*co*-AAc)-*g*-F68 (c). (D)Temperature induced absorbance change of hydrogel by UV−Vis spectrophotometry to indicate phase transition (E) Plots of I_{373}/I_{384} intensity ratio versus the logarithm of p (NIPAAm-*co*-AAc)-*g*-F68 copolymer concentration. (F) Rheological properties of the p (NIPAAm-*co*-AAc)-*g*-F68 hydrogel.

stretched bands from F68 were also observed, including the wide peak at 3366 cm^{-1} due to the stretching vibration of a hydroxyl group, and the stretching of the ether bond bands at 1116 cm^{-1}. In particular, the presence of a peak at 1113 cm^{-1} in the p(NIPAAm-*co*-AAc)-*g*-F68 spectrum was attributed to the generated ester linkage between p(NIPAAm-*co*-AAc) and F68. According to the GPC analysis results (Supporting Information Fig. S1), the M_w and M_n of p(NIPAAm-*co*-AAc)-*g*-F68 were 58,491 and 29,106, respectively, and the polymer had a PDI value of 2.0, showing unimodal distribution. Taken together, these results indicated the successful synthesis of the p (NIPAAm-*co*-AAc)-*g*-F68 copolymer.

3.2. *Formation and rheological property of nano-hydrogel*

The sol−gel transition of p(NIPAAm-*co*-AAc)-*g*-F68 was determined by the test tube inversion method. The LCST of the copolymer was determined based on the variation of its absorbance and transmittance as the temperature changed from 25 to 40 °C. As shown in Fig. 1D, the absorbance of the copolymer

solution increased sharply within the narrow temperature range of 32−34 °C. The transparent solution at 25 °C reverted into an opaque solution, and finally into a gel when the temperature was increased to 35 °C. Additionally, due to the amphiphilic structure of p(NIPAAm-*co*-AAc)-*g*-F68 copolymer, its CMC value was determined using pyrene as a hydrophobic probe. The intensity ratio I_{373}/I_{384} *vs*. log*C* changes of micelles are shown in Fig. 1E. The crossover point of the two regression lines suggests a CMC value of ∼2.6 × 10^{-3} mg/mL, indicative of its micelle stability *in vivo*. In order to examine the flow-ability of the thermo-sensitive gel, complex viscosity curves were used to characterize the degree of gel dispersion under various temperature stimuli (Fig. 1F). As shown, the values for storage modulus (G') and loss modulus (G'') were close to zero when the temperature was below 33 °C. Nevertheless, once heated above the LCST both G' and G'' began to climb dramatically, with G' always greater than G'', indicating that a gel had formed. This change can be attributed to a phase transition from a flow-able sol to a shrunken gel. Therefore, after administration *via* an intra-tumor injection, the low-viscosity thermo-sensitive gel could easily remain in the tumor tissue with ideal rheological properties.

3.3. *Preparation and characterization of TPL-loaded nano-micelles in hydrogel*

Using an optimized solvent evaporation approach, TPL was easily loaded in nano-micelles due to the amphiphilic structure and low CMC value of the p(NIPAAm-*co*-AAc)-*g*-F68 copolymer. In this TPL-loaded micelle formulation, the DLE and DEE of TPL were ∼4.52% and ∼83.52%, respectively. Both dynamic light scattering (DLS) and TEM analysis corroborated the formation of nano-micelles, as displayed in Fig. 2A and B. TPL-loaded micelles were an average of 80.87 ± 0.52 nm (PDI = 0.22), with a uniform spherical shape. Based on the sol−gel transition the copolymer exhibited at temperatures above the LCST, the TPL-loaded nano-micelle solution could form as a stable hydrogel at 37 °C. The morphology of the hydrogel was characterized by SEM (Fig. 2C). The porous structure could be observed in the cross-section of the lyophilized gel, which would be beneficial to the transportation and release of the drug from the hydrogel.

The intermolecular interaction between TPL and the hydrogel was analyzed by X-ray diffraction (XRD) and differential scanning calorimetry (DSC). As shown in Fig. 2D, a number of crystalline peaks of curcumin were observed in the 2θ range of 7−60°. These crystalline peaks became weaker in the physical mixture, due to the slight shielding provided by the copolymer hydrogel. However, these crystalline peaks were absent in TPL@nano-gel due to the presence of hydrogen-bonding interactions between TPL and the p (NIPAAm-*co*-AAc)-*g*-F68 NPs. This confirmed the amorphous or disordered-crystalline phase of TPL in the nano-gel. Additionally, in the DSC thermos-grams (Fig. 2E), TPL showed a sharp melting peak at 230 °C due to its crystalline nature. The blank hydrogel exhibited an endothermic peak at 35 °C and an exothermic peak at 142 °C. In contrast to what was observed in the mixture, the absence of a melting peak for TPL in the TPL@nano-gel indicated that changes occurred at the molecular level to prevent crystallization of TPL. These DSC results were further indication of the presence of molecular level interactions and the formation of inclusion complex in TPL@nano-gel.

To evaluate the sustained-release of TPL from the thermo-responsive hydrogel, drug release experiments were carried out at different temperatures above and below the LCST, at 37 and 25 °C, respectively. As shown in Fig. 2F, TPL loaded into a hydrogel displayed slower release kinetics than free TPL. Free TPL reached about a 90% cumulative release rate at 24 h, whereas only 74% and 53% of TPL was released from the hydrogel at 37 and 25 °C in the same time period. The 48 h drug release profiles

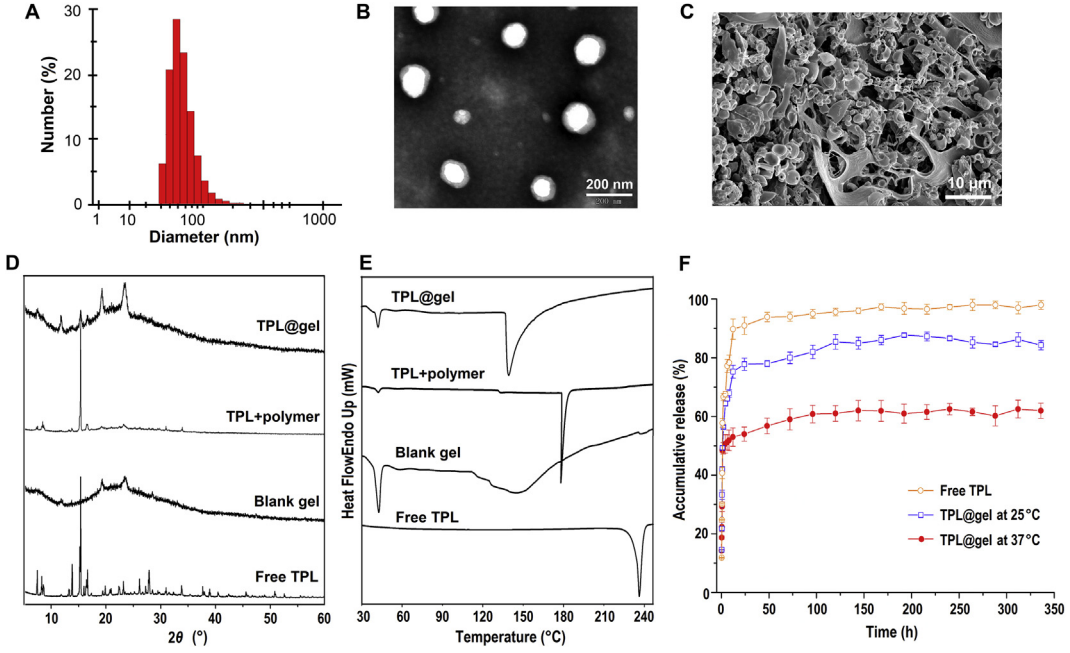

Figure 2 Characterization of TPL-loaded nano-micelles composed by p (NIPAAm-*co*-AAc)-*g*-F68 copolymer. (A) Particle distribution of nanomicelles by DLS (B) TEM image of TPL-loaded micelle solution. (C) SEM image of lyophilized hydrogel formed by sol−gel transition of micelle solution. XRD (D) and DSC (E) analysis of TPL-loaded hydrogel. (F) Cumulative release of TPL from hydrogels at 25 and 37 °C, respectively (mean ± SD, n = 3).

are shown in (Supporting Information Fig. S2). A slower release rate was observed at each time-point at 37 °C than at 25 °C, which we attributed to the formation of a polymer layer that was denser on the surface of micelles, leading to inhibited diffusion of TPL from micelles when the temperature is above the LCST. After 14 days, only about 60% of TPL was released from the gel at 37 °C. Our results indicate that when injected into a tumor, a TPL-loaded hydrogel could exhibit a sustained-release profile to promote localized treatment, along with the sol−gel transition.

3.4. *Cytotoxicity against human breast cancer cells of TPL@nano-gel*

The cytotoxicity effects of free TPL and TPL@nano-gel in MDA-MB-231 and MCF-7 human breast cancer cells were evaluated using an MTT assay. Both TPL and TPL@nano-gel induced significant cytotoxicity in breast cancer cells in a dose- and time-dependent manner (Fig. 3), whereas a control gel had no effects on the viability of those two breast cancer cell lines at any time points or dosages (Supporting Information Fig. S3). However, TPL@nano-gel exhibited higher cytotoxicity than free TPL at each concentration and time point. The IC_{50} value of MDA-MB-231 cells treated with TPL@nano-gel was 58.5 ± 8.4, 27.2 ± 5.2 and 19.5 ± 4.8 nmol/L after 48, 72 and 96 h treatments, respectively. By contrast, the respective IC_{50} values of free TPL at 48, 72 and 96 h were 128.3 ± 15.5, 72.3 ± 10.6 and 38.6 ± 7.2 nmol/L, respectively. Furthermore, the IC_{50} values of TPL@nano-gel in MCF-7 cells decreased by approximately 50%, 85% and 73% at 48, 72 and 96 h when compared to free TPL treatment at the same time points. These results revealed the stronger cytotoxicity of TPL@nano-gel than free TPL in both MDA-MB-231 and MCF-7 cells.

3.5. *MMP, apoptosis and cell cycle arrest in breast cancer cells*

To further investigate the pro-apoptotic activity of free TPL and TPL@nano-gel in human breast cancer cells, we investigated possible changes in the MMP and apoptosis rate of breast cancer cells after treatment, as loss of MMP is considered to be the initial step in triggering apoptosis. As expected, the control gel showed no effects on MMP or apoptosis rate in both MDA-MB-231 and MCF-7 breast cancer cells. As shown in Fig. 4A, after 48 h, 20 nmol/L of free TPL decreased the MMP by 16% in MDA-MB-231 cells. In contrast, 20 nmol/L of TPL@nano-gel decreased the MMP by 63%. Similarly, a significant decrease in the MMP was observed when comparing TPL@nano-gel to both the control and free TPL groups in MCF-7 cells ($P < 0.05$, Supporting Information Fig. S4).

Cell apoptosis was examined *via* an Annexin V-FITC/PI double staining assay using flow cytometry. As shown in Fig. 4B, free TPL and TPL@nano-gel markedly increased the apoptosis rates in MDA-MB-231 cells by 9.3- and 13-folds, respectively, compared to control group. After loading into the nano-micelle hydrogel, TPL exhibited significantly higher apoptosis induction activity in both MDA-MB-231 cells and MCF-7 cells (Fig. S4). These results are consistent with those obtained from the MMP assay described above and suggest that TPL@nano-gel induced superior pro-apoptotic activity compared to free TPL in both MDA-MB-231 and MCF-7 breast cancer cells.

Furthermore, as cell cycle disruption can lead to the induction of cell apoptosis as well as inhibition of cellular proliferation, cell cycle progression of breast cancer cells after treatment with free TPL or TPL@nano-gel was also investigated using PI staining. In MDA-MB-231 cells, free TPL and TPL@nano-gel treatment significantly increased the percentage of cells in the sub G1 area to

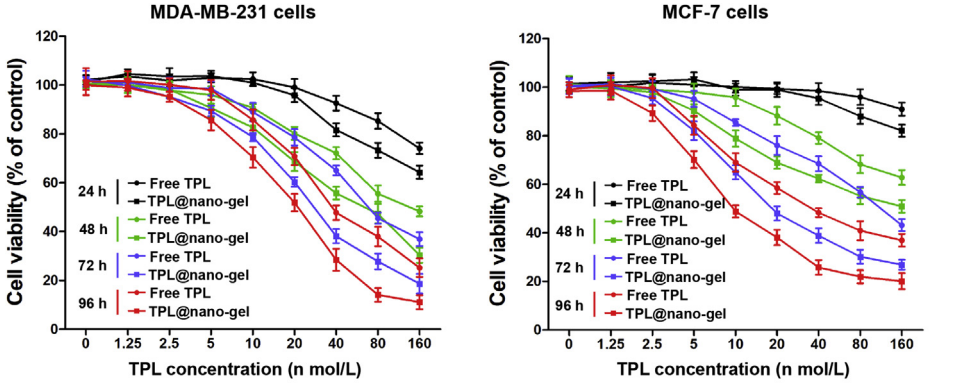

MDA-MB-231 (IC_{50} nmol/L)		
	Free TPL	TPL@nano-gel
24 h	NA	NA
48 h	128.3±15.5	58.5±8.4
72 h	72.3±10.6	27.2±5.2
96 h	38.6±7.2	19.5±4.8

MCF-7 (IC_{50} nmol/L)		
	Free TPL	TPL@nano-gel
24 h	NA	NA
48 h	>320	168.7±18.7
72 h	115.2±13.6	18.6±5.5
96 h	35.3±8.1	9.5±2.3

Figure 3 Cytotoxicity of TPL@nano-gel against MDA-MB-231 and MCF-7 human breast cancer cells, compared with free TPL. MDA-MB-231 and MCF-7 cells were treated with various concentrations of free TPL and TPL@nano-gel (0−160 nmol/L) for 24, 48, 72 and 96 h, respectively. Cell viability was assessed by MTT assay. IC_{50} values of cell viability in MDA-MB-231 and MCF-7 cells with free TPL and TPL@nano-gel treatment were calculated and analyzed by software GraphPad Prism 5.0 (mean ± SD, $n = 3$).

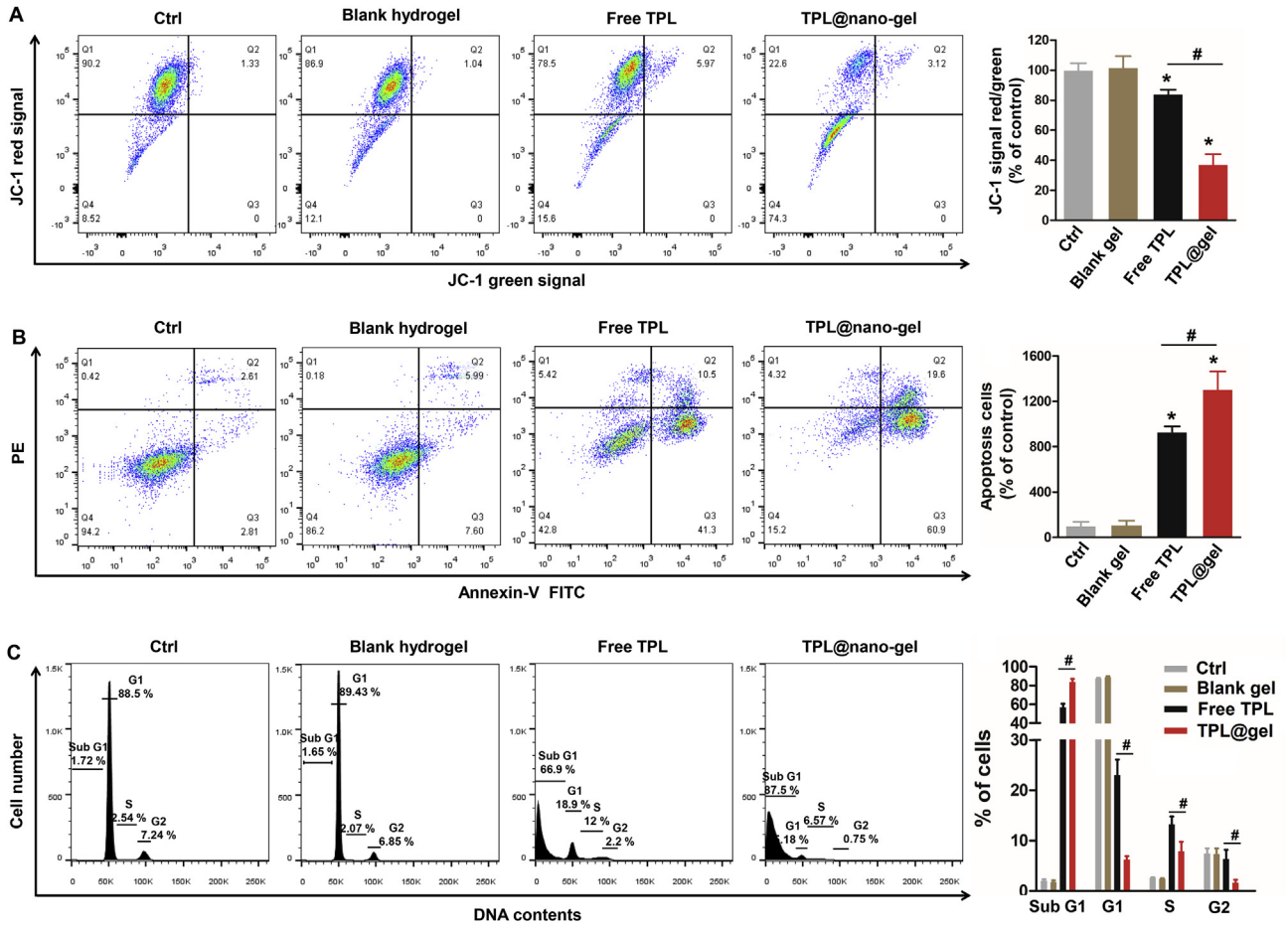

Figure 4 Effects of TPL@nano-gel on mitochondrial membrane potential (A), apoptosis (B) and cell cycle progression (C) of MDA-MB-231 cells using flow cytometry. MDA-MB-231 cells were treated with or without blank gel (160 μg/mL), or free TPL (20 nmol/L) and TPL@nano-gel (20 nmol/L) for 48 h (mean ± SD, $n = 3$). *$P < 0.05$ *versus* the control group. $^{\#}P < 0.05$ free TPL *vs.* TPL@nano-gel group.

66.9% and 87.5%, respectively, compared to 2.0% in the control group (Fig. 4C), indicating the occurrence of apoptosis. Similarly, we observed a significantly higher sub G1 population in MCF-7 cells treated with TPL@nano-gel compared to free TPL (Fig. S4). Together with the from MMP and apoptosis results, our cell cycle analysis indicates that TPL@nano-gel exhibits stronger pro-apoptosis and cell cycle arrest effects than free TPL in breast cancer cells.

3.6. *Effect on the expression of apoptosis-related protein*

To further investigate the mechanism underlying the pro-apoptotic effect of TPL@nano-gel described above, we examined the expression of apoptosis-related proteins in both MDA-MB-231 and MCF-7 breast cancer cells after treatment. In MDA-MB-231 cells, the expression of pro-apoptosis proteins including cleaved PARP, cleaved Caspase-3, cleaved Caspase-9 and Bax was significantly elevated after a 48 h TPL@nano-gel treatment compared to the control, and were also elevated compared to the free TPL treatment (Fig. 5A). Similarly, both free TPL and TPL@nano-gel significantly increased the expression of cleaved PARP, cleaved Caspase-3, cleaved Caspase-9, and Bax, and decreased the expression of Bcl-2 in MCF-7 cells, with TPL@nano-gel inducing higher upregulation of these proteins than free TPL (Fig. 5B). Based on the regulation of these pro-apoptotic proteins, the apoptosis promoted by TPL@nano-gel would be connected to the endogenous apoptosis mediated by mitochondria pathways.

Additionally, cyclin D1 is an important protein responsible for cell cycle regulation. Disruption of cyclin D1 is likely to induce cell cycle arrest, while further inhibiting cell proliferation and triggering cell apoptosis. Western blot analysis showed that both free TPL and TPL@nano-gel caused a significant decrease in cyclin D1 protein levels in MDA-MB-231 and MCF-7 cells compared to the control group. Compared with free TPL, TPL@nano-gel exhibited a greater down-regulation of cyclin D1 expression.

3.7. *Effect on caspase 3/7 and VEGF activity in cancer cells*

We further examined caspase-3/7 activity in MDA-MB-231 and MCF-7 cells using a commercial kit. As shown in Fig. 5C, TPL@nano-gel treatment significantly increased the caspase-3/7 activity 4.29- and 2.85-folds in MDA-MB-231 and MCF-7 cells, respectively, compared to the control group, and also caused a greater increase than treatment with free TPL. These data are consistent with the expression levels of caspase proteins analyzed by Western blot.

Many tumor cells are able to secret VEGF into the tumor microenvironment to initiate angiogenesis in order to increase

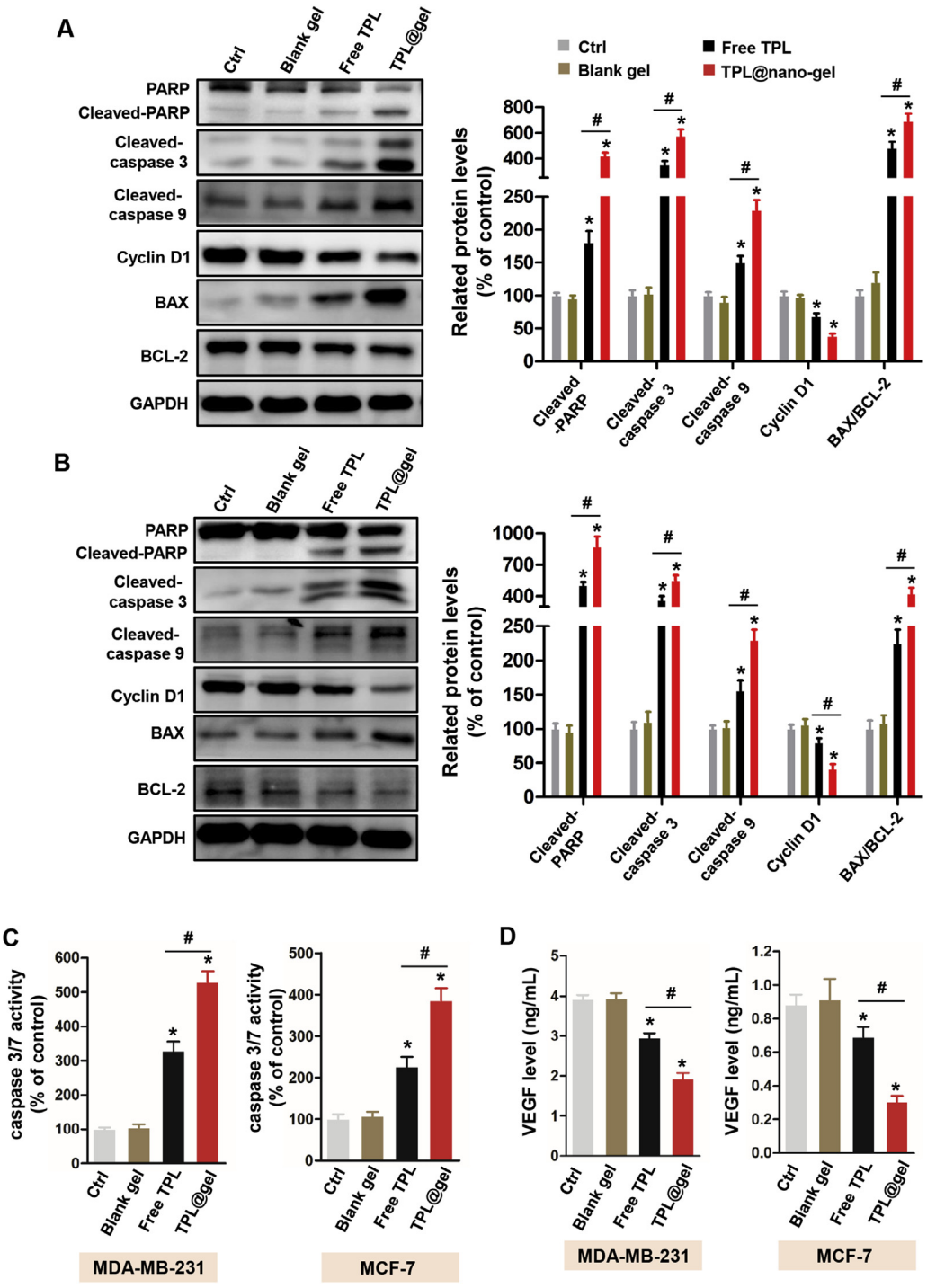

Figure 5 Effects of TPL@nano-gel on the expression levels of proteins related to apoptosis in MDA-MB-231 (A) and MCF-7 (B) breast cancer cells after 48 h treatment by Western blot analysis. Proteins were involved in the regulation of apoptosis including PARP, cleaved-PARP, cleaved-Caspase 3, cleaved-Caspase 9, Cyclin D1, Bax and Bcl-2. VEGF levels in the culture medium of MDA-MB-231 and MCF-7 cells after 48 h treatment of various agents were measured by a commercial VEGF ELISA kit (C). Caspase 3/7 activity in MDA-MB-231 and MCF-7 cells after 48 h treatment was measured by a commercial Caspase 3/7 activity kit (D). $^{*}P < 0.05$ *vs.* the control group. $^{\#}P < 0.05$ TPL@gel *versus* free TPL group (mean ± SD, $n = 3$).

their oxygen and nutrient supply. Therefore, we further investigated the inhibitory effects of TPL on VEGF secretion in MDA-MB-231 and MCF-7 breast cancer cells. As shown in Fig. 5D, the extracellular VEGF level decreased in MDA-MB-231 and MCF-7 cells after treatment with either free TPL or TPL@nano-gel. In comparison with free TPL, TPL@nano-gel caused a decrease in VEGF secretion of approximately 36% and 57% in MDA-MB-231 and MCF-7 cells, respectively. These data suggest that TPL@nano-gel treatment could potentially inhibit angiogenic activity in tumors.

3.8. TPL@nano-gel inhibited HUVEC proliferation, migration and invasion

As reported previously, vascular endothelial cell proliferation, migration, and invasion are critical steps in angiogenesis. We explored the effects of TPL at non-cytotoxic concentrations on HUVEC proliferation. As shown in Fig. 6A, non-significant cytotoxic effects on HUVEC proliferation could be observed when the concentration of TPL was below 20 nmol/L. However, treatment with TPL formulations for 48 h induced remarkable cell proliferation suppression at 40 nmol/L of TPL, indicating that only concentrations below 40 nmol/L of TPL could be employed in follow-up studies. HUVECs were synchronized by starvation for 24 h, and then stimulated by VEGF (20 ng/mL) in the absence or presence of TPL (1.25−20 nmol/L) for another 48 h. Using MTT assays, we observed significantly reduced cell viability in

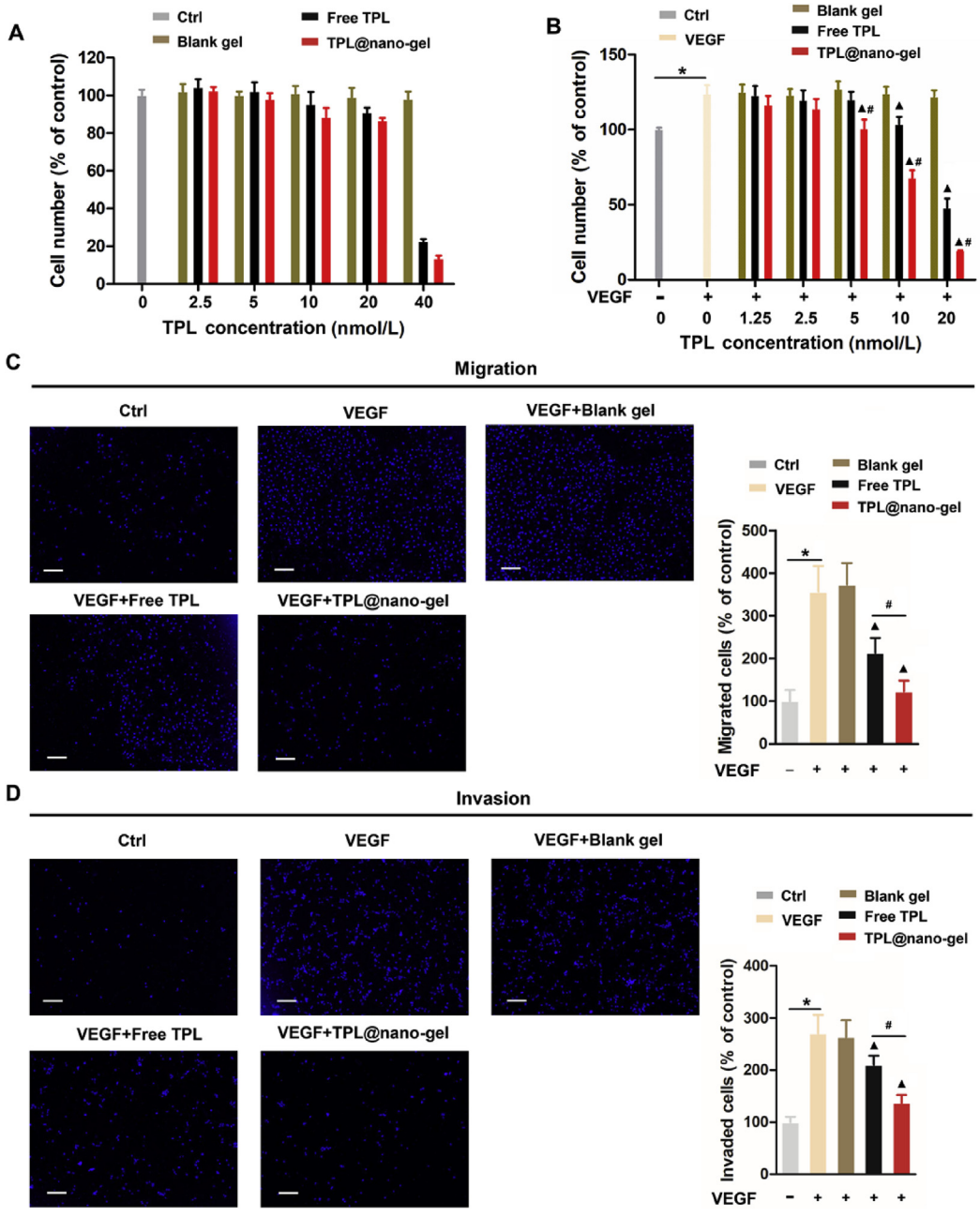

Figure 6 TPL@nano-gel inhibited VEGF-induced HUVEC cell proliferation, migration, and invasion. (A) HUVECs treated with blank gel, free TPL and TPL@nano-gel (0−40 nmol/L) for 48 h and then cell viability was measured by MTT assay. (B) HUVECs were pre-starved in low serum medium for 24 h, then treated without (control) or with VEGF (20 ng/mL) in the presence of blank gel, free TPL and TPL@nano-gel (0−20 nmol/L) for 48 h. Cell viability was measured by MTT assay. Endothelial cell transwell migration (C) and invasion (D) were studied after 24 h treatment of various agents with TPL at 10 nmol/L in the presence of VEGF (20 ng/mL). HUVECs received VEGF (20 ng/mL) treatment served as positive control. Scale bar is 200 μm, $^{*}P < 0.05$, positive control with VEGF stimulation *versus* negative control group, $^{\blacktriangle}P < 0.05$, TPL formulations *versus* positive control with VEGF stimulation, and $^{\#}P < 0.05$, TPL@nano-gel *vs.* free TPL group (mean ± SD, $n = 3$).

VEGF-stimulated HUVECs treated with TPL formulations in a dose-dependent manner, with TPL@nano-gel exhibiting more prominent effects than free TPL (Fig. 6B). The suppression of VEGF-induced angiogenesis by TPL@nano-gel was further investigated using Transwell migration and invasion assays. As expected, when introduced to the chemoattractant VEGF, an increased number of migrating and invading cells passed through the gelation-coated Transwell membrane barrier. At a TPL concentration of 10 nmol/L, TPL@nano-gel displayed higher inhibition effects on HUVEC migration (Fig. 6C) and invasion (Fig. 6D) compared to free TPL, indicating that TPL@nano-gel could effectively suppress VEGF-induced angiogenesis *in vitro*.

3.9. *TPL@nano-gel inhibited VEGFR-2 signaling in VEGF-stimulated HUVECs*

The VEGF/VEGFR-2 signaling pathway plays a central role in the regulation of tumor angiogenesis. To further investigate the underlying anti-angiogenic mechanisms of free TPL and TPL@nano-gel, we used Western blotting to analyze the expression of proteins involved in the VEGFR-2 mediated signaling pathway. As shown in Fig. 7, VEGF (50 ng/mL) significantly upregulated phospho-VEGFR2 in HUVECs. Both free TPL and TPL@nano-gel markedly downregulated VEGF-induced phosphorylation of VEGFR2, with TPL@nano-gel exhibiting a more severe downregulation than free TPL. Moreover, downstream proteins involved in VEGFR-2 signaling, including AKT, ERK1/2, P38 and eNOS, were also significantly activated, *via* phosphorylation, by VEGF stimulation. TPL@nano-gel significantly inhibited the activation of these proteins. These results demonstrated that TPL@nano-gel induced anti-angiogenic activities, possibly mediated by the inhibition of the VEGFR-2 angiogenesis signal pathway.

3.10. *TPL@nano-gel inhibited microvessel sprouting ex vivo*

We further performed an *ex vivo* rat aortic ring sprouting assay to analyze the anti-angiogenic capabilities of TPL@nano-gel. As shown in Fig. 8A, VEGF-A (25 ng/mL) induced significant sprouting of micro-vessels to form a complex network around the aortic rings. However, treatment with TPL formulations (20 nmol/L) significantly reduced VEGF-induced micro-vessel sprouting. In particular, TPL@nano-gel was able to completely suppress sprouting of micro-vessels, while the control gel displayed no inhibition activity. This result indicates that TPL@nano-gel is an effective suppressor of VEGF-induced angiogenesis *ex vivo*.

Next, a matrigel plug assay was used to investigate the *in vivo* antiangiogenic activity of TPL@nano-gel. As shown in Fig. 8B, the matrigel plugs treated with VEGF alone were dark red in color. In contrast, plugs treated with TPL@nano-gel together with VEGF were light red color, indicating a substantial decrease in micro-vessel formation compared to the VEGF-only plugs. The hemoglobin content in TPL@nano-gel samples decreased by

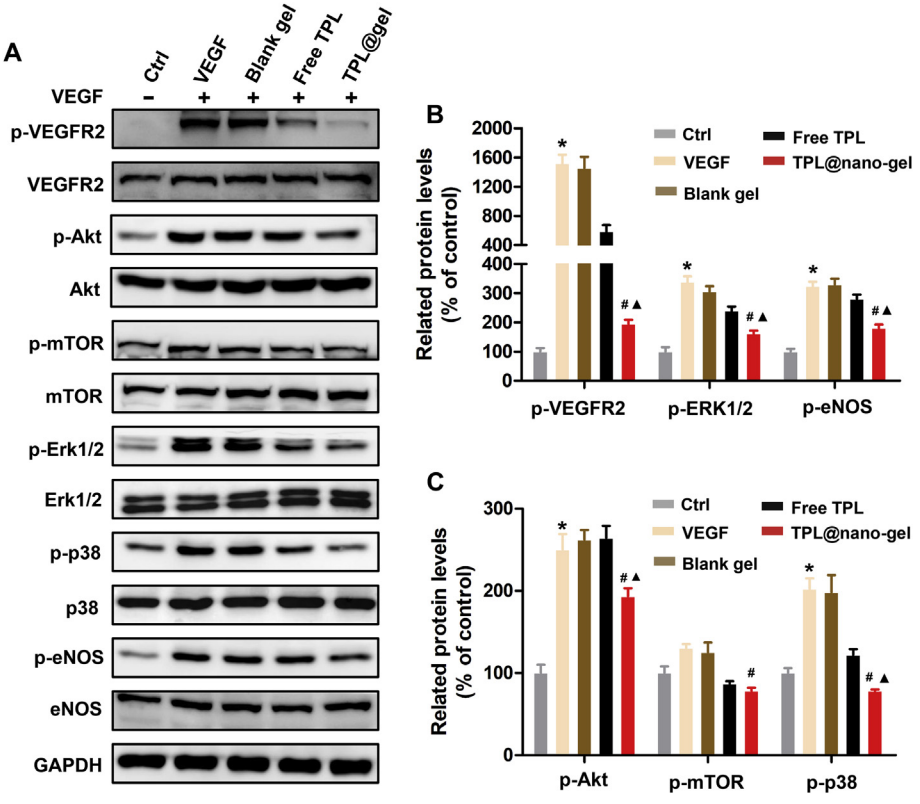

Figure 7 Effects of TPL@nano-gel on VEGFR-2 mediated angiogenesis signaling pathway. HUVECs were starved in low serum medium for 3 h and then treated with TPL formulations at 10 nmol/L for 24 h, followed by stimulation of VEGF (50 ng/mL) for 15 min. The expression levels of the major proteins involved in VEGFR2-mediated angiogenesis pathway such as VEGFR2, p-VEGFR2, AKT, p-AKT, mTOR, p-mTOR, ERK1/2, p-ERK1/2, P38, p-P38, eNOS and p-eNOS were detected by Western blot analysis (A). Quantitative analysis of the protein expression levels in HUVECs (B, C). $^{*}P < 0.05$, positive control with VEGF stimulation *vs.* negative control group; $^{\blacktriangle}P < 0.05$, TPL formulations *vs.* positive control with VEGF stimulation; $^{\#}P < 0.05$, TPL@nano-gel *vs.* free TPL group (mean ± SD, $n = 3$).

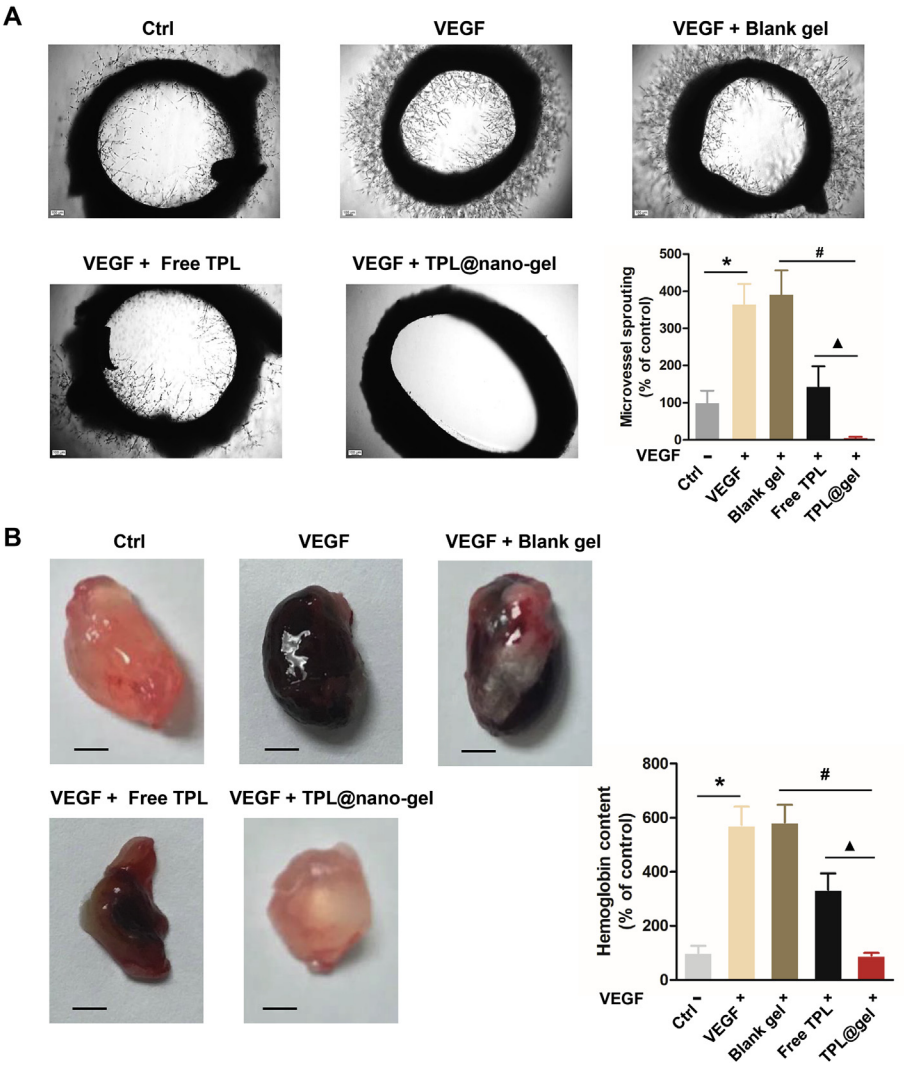

Figure 8 TPL@nano-gel inhibited angiogenic activity of aorta ring sprouting *ex vivo* and VEGF-induced angiogenesis matrigel plug *in vivo*. (A) Representative photographs of micro-vessel sprouting in rat aortic rings. Rat aortic rings were embedded in matrigel and treated with TPL formulations with 20 nmol/L of TPL in the presence of VEGF (100 ng/mL) for 10 days. Then the micro-vessel growth was recorded by an inverted microscope and the number of micro-vessel sprouting was quantified by ImageJ software. Aortic rings VEGF (100 ng/mL) served as positive control. Scale bar = 100 μm. Quantitative analysis of micro-vessel sprouting in each group. (B) Representative photographs of blood vessels formation in matrigel plugs. 6-Week-old BALB/c male mice were subcutaneously injected with 0.5 mL of growth factor-reduced matrigel containing VEGF (250 ng) and heparin (100 Unit) with TPL formulations with 20 nmol/L of TPL. After 14 days, the animals were sacrificed and the matrigel plugs were removed, photographed and weighted. Scale bar: 2.5 mm. To quantify the formation of functional blood vessels, the amount of hemoglobin was measured using the Drabkin reagent Kit (mean ± SD, $n = 3$), $^{*}P < 0.05$, VEGF alone group *vs.* the control group, $^{\#}P < 0.05$, TPL@nano-gel *vs.* blank gel, and $^{\blacktriangle}P < 0.05$, TPL@gel *vs.* free TPL group.

86.4%, compared to VEGF-only samples. Therefore, TPL@nano-gel exhibited marked antiangiogenic capacity *in vivo*.

3.11. *Long-term intra-tumoral retention of hydrogel*

First, we used a Cy5-loaded nano-micelle system in order to monitor the *in vivo* tumoral retention of the hydrogel through a real-time and noninvasive manner[23] by introducing Cy5 loaded in the nano-micelles system, based on the preparation method of TPL@nano-gel. As shown in Fig. 9, after injected into tumors, the free Cy5 suspension solution was cleared rapidly. After 8 h post-injection, only a small amount of free Cy5 could be observed in tumor tissue, which exhibited the dramatically declined profile alone with time. And the fluorescence derived from free Cy5 can be scarcely observed at 72 h. However, Cy5-loaded micelle solution rapidly converted into a gel state, displaying the centralized fluorescence in the tumor. As the time went by, unlike the rapidly decayed fluorescence in free Cy5 group, Cy5-labled gel stayed strong fluorescence intensity during the whole 72 h period. Furthermore, to clearly characterize the fluorescence distribution in main organs, the *ex vivo* fluorescent images of the dissected organs from the sacrificed tumor-bearing mice at both 24 and 48 h after intra-tumoral injection were also shown. In contrast to less fluorescence in free Cy5 group, the strong fluorescence can be

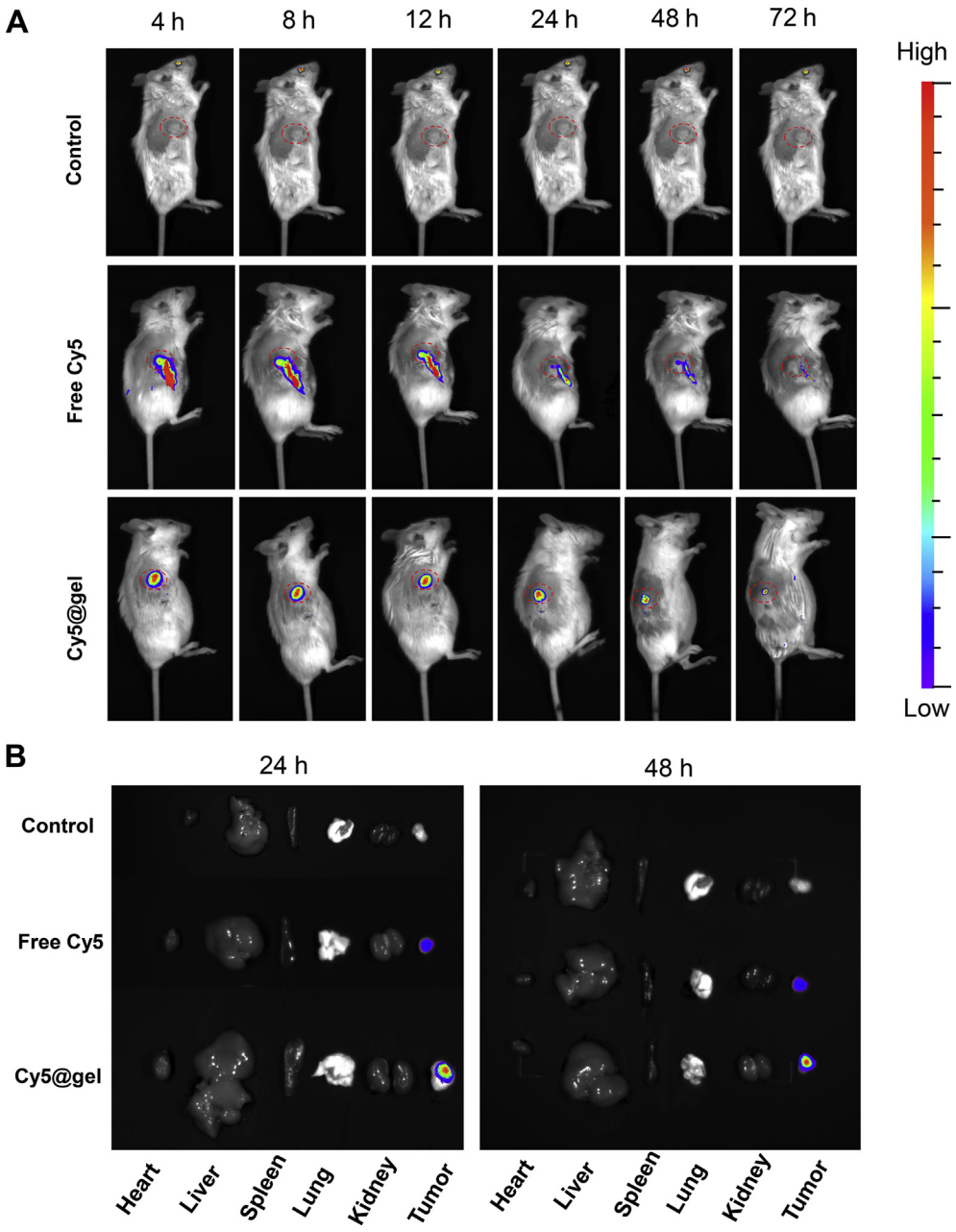

Figure 9 Retention of free Cy5 and Cy5-labled gel in tumor observed by IVIS spectrum. (A) Fluorescent images of the retention of Cy5 formulations in tumors after intra-tumoral injection at predetermined time intervals, *i.e.*, 4, 8, 12, 24, 48 and 72 h after injection (B) Images of dissected organs of the mice treated with Cy5 formulations for 24 and 48 h post-injection.

observed only in tumor tissue of mice administrated by Cy5@nano-gel at 72 h post-injection, indicating its long retention in the tumor tissue.

3.12. TPL@nano-gel inhibited tumor growth and prolonged survival rate in vivo

We evaluated the *in vivo* therapeutic efficacy of TPL@nano-gel by intra-tumoral injection into 4T1 tumor-bearing nude mice (once every 4 day at a 0.45 mg/kg TPL-equivalent dose). On Days 14, 6 mice in each group were sacrificed. As shown in Fig. 10A–D, after three consecutive injections, TPL@nano-gel showed a greater therapeutic effect in the inhibition of tumor growth than other formulations. After 14 days, the tumor volume increase in mice treated with TPL@nano-gel was much lower than that of the other treatment groups. Furthermore, compared with the sharp body weight decline induced by free TPL, there was no significant body weight decrease observed in the TPL@nano-gel group, indicating it caused minimal side effect. Additionally, using an absolute tumor volume threshold as a surrogate marker for survival, the TPL@nano-gel treatment also resulted in extended survival time relative to other groups, as seen in the Kaplan−Meier survival curve[24]. As shown in Fig. 10E, the median survival time of the saline group, control gel group, and free TPL group was 14, 16 and 22 days, respectively. Notably, less than 20% of mice treated with TPL@nano-gel died over the course of 36 days,

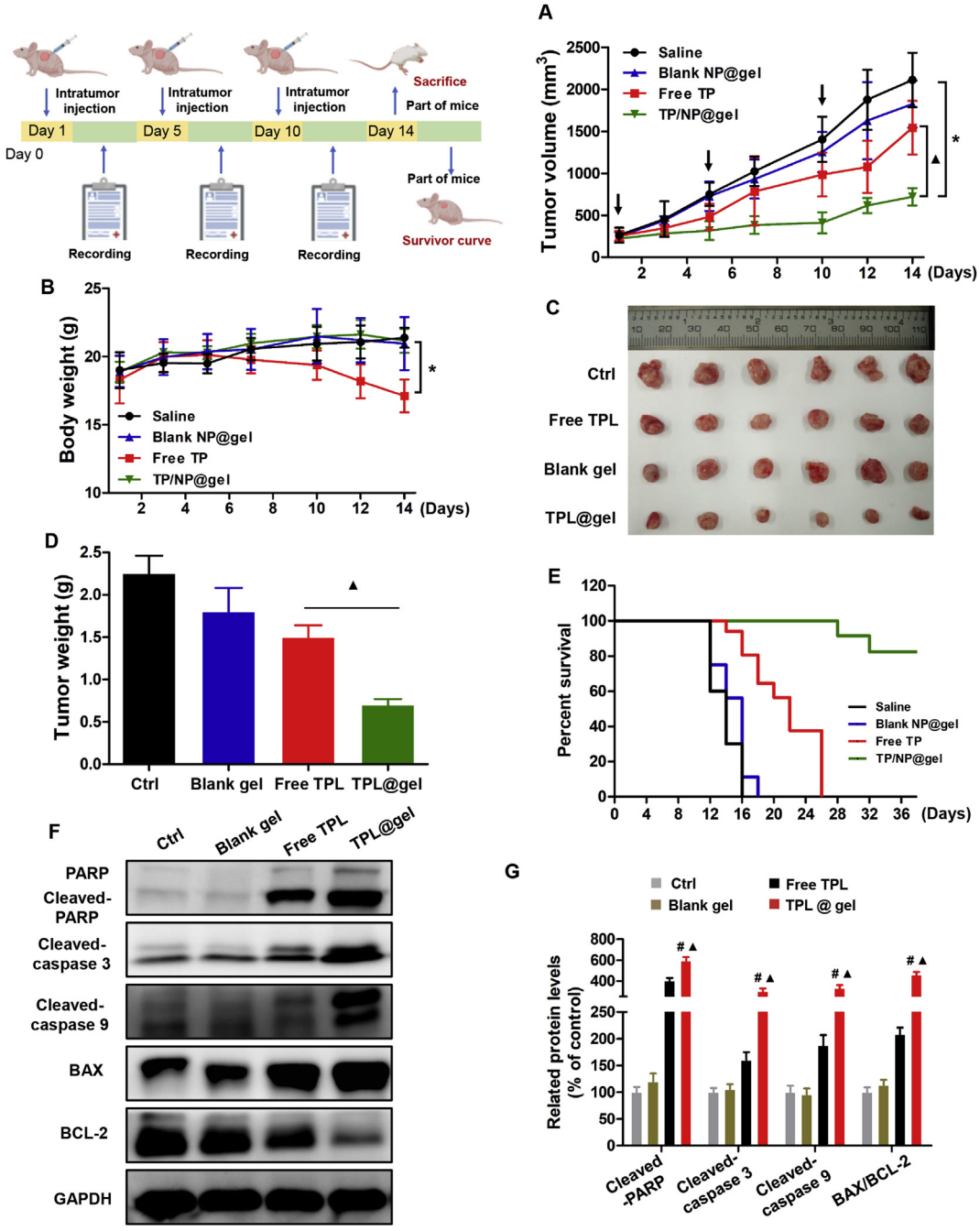

Figure 10 *In vivo* anticancer activity of TPL@nano-gel on 4T1 xenograft model. Tumor volume changes (A), body weight changes (B), Photographs of tumors (C), final mean tumor weights (D), Kaplan−Meier survival curve (E) of mice receiving the above-indicated treatments. Expressions of apoptosis-related proteins in tumor tissue by Western Blot analysis (F). Quantitative analysis of those apoptosis-related protein expressions (G) (mean ± SD, $n = 3$), $^{*}P < 0.05$ *versus* the control group; $^{\#}P < 0.05$, TPL@nano-gel *vs.* blank gel; and $^{\blacktriangle}P < 0.05$, TPL@nano-gel *vs.* free TPL group.

demonstrating that loading TPL into a nano-gel could significantly increase both its anticancer efficacy and safety. Based on our previous observations that TPL induced apoptosis mediated by mitochondria pathways *in vitro*, we evaluated the expression of several apoptosis-related proteins in tumors of mice treated with different TPL formulations. As shown in Fig. 10F and G, cleaved PARP, cleaved caspase-3, cleaved caspase-9 and BAX were significantly upregulated by TPL formulations, whereas the expression of the anti-apoptotic protein BCL-2 was strongly inhibited. TPL@nano-gel exhibited the highest degree of upregulation of pro-apoptosis signal pathway proteins compared to the other treatment groups.

After mice were sacrificed, we performed histological analysis on tumor, liver, and kidney samples using H&E staining to evaluate the systemic side effects after different treatments. As shown in Fig. 11, cells in tumor tissues were tightly packed within the stroma, and necrosis or apoptotic cells were rarely observed in the saline group. However, after treatment with different TPL

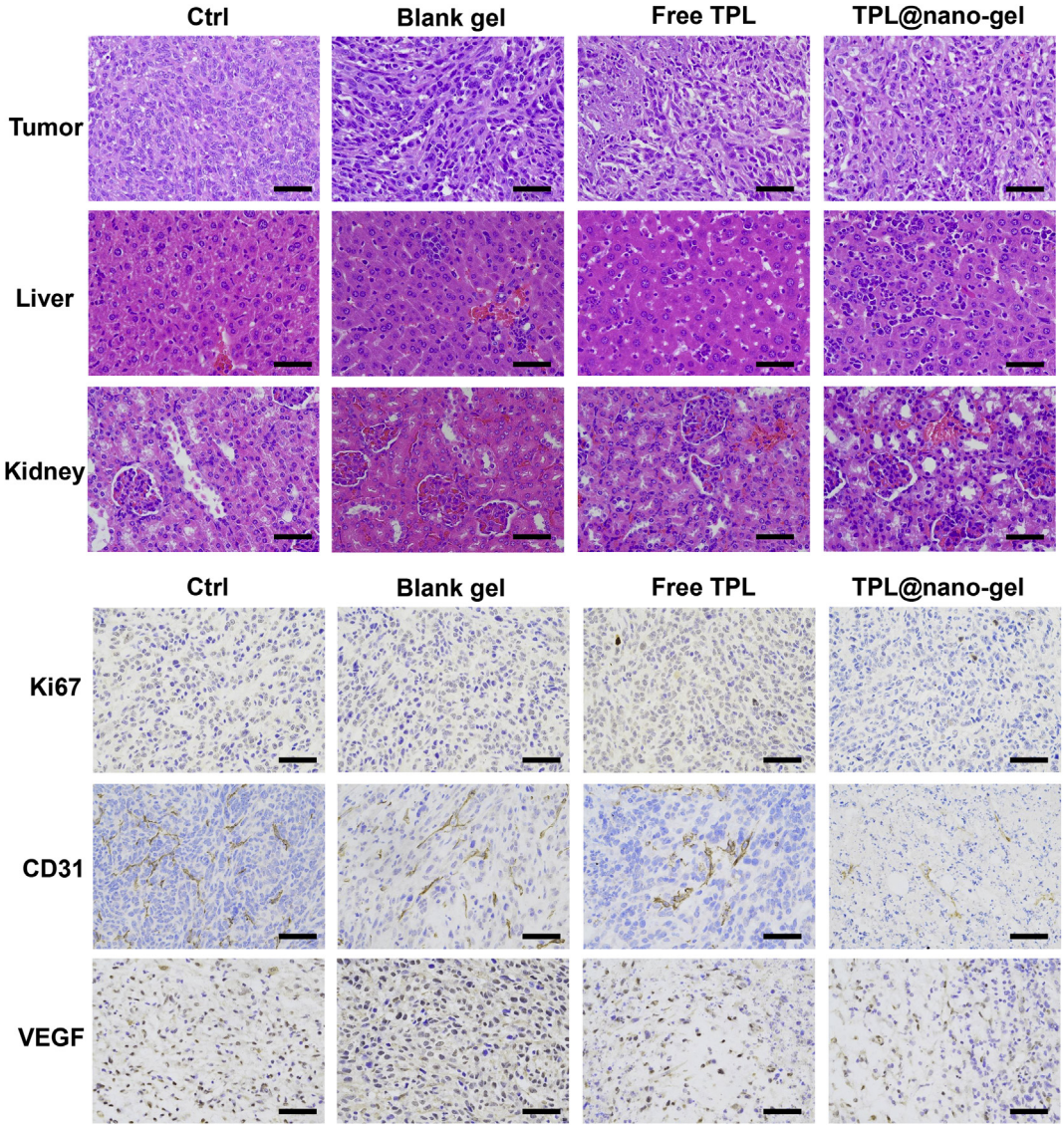

Figure 11 Representative histological microphotographs of tumor, liver, kidney of mice receiving the above-indicated treatments by H&E staining, and tumor tissues by immunohistochemical staining with primary antibodies against Ki-67, CD31, and VEGF. Scale bar = 100 μm.

formulations, extensive shrinkage, fragmentation and loss of nuclei were observed in tumor tissues. Moreover, H&E analysis on liver and kidney samples revealed no obvious tissue abnormality or damage in mice treated with TPL@nano-gel, indicating that there were no noticeable histological changes. In contrast, in mice treated with free TPL, hepatotoxicity, as evidenced by liver damage and cellular edema, was clearly observed. Moreover, to confirm the enhanced pro-apoptotic and anti-angiogenic activities of TPL@nano-gel *in vivo,* the expression of Ki-67 (a cellular marker for cell proliferation), and VEGF and CD31 (markers for neo-vasculature) in tumor tissues was evaluated by immunohistochemical staining. We observed an abundance of blood vessels in the saline group. Treatment with free TPL caused a slight decrease in the number of blood vessels in the tumor tissue, whereas treatment with TPL@nano-gel strongly inhibited neovascularization. These results provided further evidence of the low systemic toxicity and enhanced anticancer efficacy of TPL@nano-gel, and supported its involvement in promoting apoptosis and suppressing angiogenesis.

4. Conclusion

In this study, we developed a thermo-responsive hydrogel formed by the sol−gel transition of nano-micelles composed of self-assembled, synthesized amphiphilic p(NIPAAm-*co*-AAc)-*g*-F68 copolymer for the sustained release of TPL in the localized treatment of breast cancer. Along with gelatinization at temperatures above the LCST, the TPL in the nano-gel was released in a slow and sustained manner over 14 days. *In vitro* cytotoxicity experiments confirmed the enhanced anticancer effect of this TPL-loaded gel against breast cancer cells, and indicated that this is related to the upregulation of cell apoptosis pathways. Additionally, upon loading into the gel, TPL exhibited prominent anti-angiogenesis activities, including inhibiting VEGF-induced HUVEC migration and invasion *in vitro*, inhibiting VEGF-induced micro-vessel sprouting *ex vivo*, and preventing VEGF-induced neovascularization *in vivo* as determined by matrigel plug assay. Our work revealed that the anti-angiogenesis effects were mediated by inhibition of VEGFR-2 signaling, which

combined with the induction of apoptosis to promote "two strikes" against tumor cells. Intra-tumoral injection of TPL@nano-gel, at a low TPL dosage of 0.45 mg/kg, into 4T1 tumor-bearing mice three times over 14 days, effectively induced tumor shrinkage. Meanwhile, the administration of TPL@nano-gel was able to remarkably extend the survival rate and reduce side-effects, as compared to free TPL. Therefore, this injectable thermo-responsive hydrogel may be a useful delivery system for TPL, allowing for long-term delivery and low risk.

Acknowledgments

The authors are grateful for the financial support from the National Natural Science Foundation of China (Grant Nos. 81973662 and 8170371), Scientific Development Program of Sichuan Province (2019JDJQ0049, China), China Postdoctoral Science Foundation (Grant Nos. 2017M612930 and 2019T120817), and Young Elite Scientists Sponsorship Program by CAST (2018QNRC1-01, China). The authors also appreciate a native English speaker from an editing company to edit this manuscript thoroughly.

Author contributions

Jinming Zhang and Chaomei Fu designed the research. Yaoyao Luo and Jingjing Li carried out the experiments and performed data analysis. Yichen Hu and Fei Gao participated part of the experiments. Funeng Geng provided experimental drugs and quality control. Jinming Zhang and Yaoyao Luo wrote the manuscript. George Pak-Heng Leung revised the manuscript. All of the authors have read and approved the final manuscript.

Conflicts of interest

The authors have no conflicts of interest to declare.

Appendix A. Supporting information

Supporting data to this article can be found online at https://doi.org/10.1016/j.apsb.2020.05.011.

References

1. Hou W, Liu B, Xu H. Triptolide: medicinal chemistry, chemical biology and clinical progress. *Eur J Med Chem* 2019;**176**:378−92.
2. Meng C, Zhu H, Song H, Wang Z, Huang G, Li D, et al. Targets and molecular mechanisms of triptolide in cancer therapy. *Chin J Canc Res* 2014;**26**:622−6.
3. Liu H, Shen M, De Ru D, Duan Y, Ding C, et al. The effect of triptolide-loaded exosomes on the proliferation and apoptosis of human ovarian cancer SKOV3 cells. *BioMed Res Int* 2019;**2019**: 2595801.
4. Zhang Y, Zhang J, Chen M, Gong H, Thamphiwatana S, Eckmann L, et al. Nanoparticle–hydrogel: a hybrid biomaterial system for localized drug delivery. *ACS Appl Mater Interfaces* 2016;**44**:2049−61.
5. Deng H, Dong A, Song J, Chen X. Injectable thermosensitive hydrogel systems based on functional PEG/PCL block polymer for local drug delivery. *J Control Release* 2019;**297**:60−70.
6. Norouzi M, Nazari B, Miller DW. Injectable hydrogel-based drug delivery systems for local cancer therapy. *Drug Discov Today* 2016; **21**:1835−49.
7. Yang W, Zhou P, Liang L, Cao Y, Qiao J, Li X, et al. Nanogel-incorporated injectable hydrogel for synergistic therapy based on sequential local delivery of combretastatin-A4 phosphate (CA4P) and doxorubicin (DOX). *ACS Appl Mater Interfaces* 2018;**10**:18560−73.
8. Gaowa A, Horibe T, Kohno M, Sato K, Harada H, Hiraoka M, et al. Combination of hybrid peptide with biodegradable gelatin hydrogel for controlled release and enhancement of anti-tumor activity *in vivo*. *J Control Release* 2014;**176**:1−7.
9. Lai WF, He ZD. Design and fabrication of hydrogel-based nanoparticulate systems for *in vivo* drug delivery. *J Control Release* 2016; **243**:269−82.
10. Zhao X, Liu X, Zhang P, Liu Y, Ran W, Cai Y, et al. Injectable peptide hydrogel as intraperitoneal triptolide depot for the treatment of orthotopic hepatocellular carcinoma. *Acta Pharm Sin B* 2019;**9**: 1050−60.
11. Alexander A, Ajazuddin, Khan J, Saraf S, Saraf S. Polyethylene glycol (PEG)-poly(*N*-isopropylacrylamide) (PNIPAAm) based thermosensitive injectable hydrogels for biomedical applications. *Eur J Pharm Biopharm* 2014;**88**:575−85.
12. Das D, Ghosh P, Ghosh A, Haldar C, Dhara S, Panda AB. Stimulus-responsive,biodegradable, biocompatible, covalently cross-linked hydrogel based on dextrin and poly(*N*-isopropylacrylamide) for *in vitro/in vivo* controlled drug release. *ACS Appl Mater Interfaces* 2015;**7**:14338−51.
13. Ma C, Shi Y, Pena DA, Peng L, Yu G. Thermally responsive hydrogel blends: a general drug carrier model for controlled drug release. *Angew Chem Int Ed Engl* 2015;**54**:7376−80.
14. Zhang K, Wang Z, Li Y, Jiang Z, Hu Q, Liu M, et al. Dual stimuli-responsive *N*-phthaloylchitosan-graft-(poly(*N*-isopropylacrylamide)-block-poly(acrylic acid)) copolymer prepared *via* RAFT polymerization. *Carbohydr Polym* 2013;**92**:662−7.
15. Liu M, Song X, Wen Y, Zhu J, Li J. Injectable thermoresponsive hydrogel formed by alginate-*g*-poly(*N*-isopropylacrylamide) that releases doxorubicin-encapsulated micelles as a smart drug delivery system. *ACS Appl Mater Interfaces* 2017;**9**:35673−82.
16. Shen W, Luan J, Cao L, Sun J, Yu L, Ding J. Thermogelling polymer-platinum(IV) conjugates for long-term delivery of cisplatin. *Biomacromolecules* 2015;**16**:105−15.
17. Wang W, Deng L, Liu S, Li X, Zhao X, Hu R. Adjustable degradation and drug release of a thermosensitive hydrogel based on a pendant cyclic ether modified poly(epsilon-caprolactone) and poly(ethylene glycol)co-polymer. *Acta Biomater* 2012;**8**:3963−73.
18. Agarwal P, Rupenthal ID. Injectable implants for the sustained release of protein and peptide drugs. *Drug Discov Today* 2013;**18**: 337−49.
19. Wang Y, Wang J, Yuan Z, Han H, Li T, Li L. Chitosan cross-linked poly(acrylic acid) hydrogels: drug release control and mechanism. *Colloids Surf B Biointerfaces* 2017;**152**:252−9.
20. Li R, Li Y, Wu Y, Zhao Y, Chen H, Yuan Y, et al. Heparin-poloxamer thermosensitive hydrogel loaded with bFGF and NGF enhances peripheral nerve regeneration in diabetic rats. *Biomaterials* 2018;**168**: 24−37.
21. Shieh YT, Lin PY, Chen T, Kuo SW. Temperature-, pH- and CO_2-sensitive poly(*N*-isopropylacryl amide-*co*-acrylic acid) copolymers with high glass transition temperatures. *Polymers* 2016;**8**:434.
22. Wang W, Yu W. Preparation and characterization of CS-*g*-PNIPAAm microgels and application in a water vapour-permeable fabric. *Carbohydr Polym* 2015;**127**:11−8.
23. Li B, Liu P, Wu H, Xie X, Chen Z, Zeng F. A bioorthogonal nanosystem for imaging and *in vivo* tumor inhibition. *Biomaterials* 2017; **138**:57−68.
24. Gao C, Liang J, Zhu Y, Ling C, Cheng Z, Li R, et al. Menthol-modified casein nanoparticles loading 10-hydroxycamptothecin for glioma targeting therapy. *Acta Pharm Sin B* 2019;**9**:843−57.
25. Fathi M, Alami-Milani M, Geranmayeh MH, Barar J, Erfan-Niya H, Omidi Y. Dual thermo-and pH-sensitive injectable hydrogels of chitosan/(poly(*N*-isopropylacrylamide-*co*-itaconic acid)) for doxorubicin delivery in breast cancer. *Int J Biol Macromol* 2019;**128**:957−64.
26. Song C, Yu S, Liu C, Deng Y, Xu Y, Chen X, et al. Preparation of thermo-responsive graft copolymer by using a novel macro-RAFT

agent and its application for drug delivery. *Mater Sci Eng C Mater Biol Appl* 2016;**62**:45−52.
27. Wei W, Hu X, Qi X, Yu H, Liu Y, Li J, et al. A novel thermo-responsive hydrogel based on salecan and poly(*N*-isopropylacrylamide): synthesis and characterization. *Colloids Surf B Biointerfaces* 2015;**125**:1−11.
28. Leal D, De Borggraeve W, Encinas MV, Matsuhiro B, Müller R. Preparation and characterization of hydrogels based on homopolymeric fractions of sodium alginate and PNIPAAm. *Carbohydr Polym* 2013;**92**:157−66.
29. Gao W, Hu Y, Xu L, Liu M, Wu H, He B. Dual pH and glucose sensitive gel gated mesoporous silica nanoparticles for drug delivery. *Chin Chem Lett* 2018;**29**:107−10.
30. Wang T, Ding Y, Yang Y, Wang Z, Gao W, Li D, et al. Synergistic antitumour effects of triptolide plus 10-hydroxycamptothecin onbladder cancer. *Biomed Pharmacother* 2019;**115**:108899.
31. Zhang J, Li J, Shi Z, Yang Y, Xie X, Lee SM, et al. pH-sensitive polymeric nanoparticles for co-delivery of doxorubicin and curcumin to treat cancer *via* enhanced pro-apoptotic and anti-angiogenic activities. *Acta Biomater* 2017;**58**:349−64.
32. Lien J, Chung C, Huang T, Chang T, Chen K, Gao G, et al. A novel 2-aminobenzimidazole-based compound Jzu 17 exhibits anti-angiogenesis effects by targeting VEGFR-2 signalling. *Br J Pharmacol* 2019;**176**:4034−49.
33. Li Y, Wu Y, Huang L, Miao L, Zhou J, Satterlee AB, et al. Sigma receptor-mediated targeted delivery of anti-angiogenic multifunctional nanodrugs for combination tumor therapy. *J Control Release* 2016;**228**:107−19.
34. Ruan S, Cao X, Cun X, Hu G, Zhou Y, Zhang Y, et al. Matrix metalloproteinase-sensitive size-shrinkable nanoparticles for deep tumor penetration and pH triggered doxorubicin release. *Biomaterials* 2015;**60**:100−10.